FILTERING RANDOM LAYERING EFFECTS IN IMAGING

L. BORCEA†, F. GONZÁLEZ DEL CUETO†, G. PAPANICOLAOU‡, AND C. TSOGKA§

Abstract. Objects that are buried deep in heterogeneous media produce faint echoes which are difficult to distinguish from the backscattered field. Sensor array imaging in such media cannot work unless we filter out the backscattered echoes and enhance the coherent arrivals that carry information about the objects that we wish to image. We study such filters for imaging in strongly backscattering, finely layered media. The fine layering is unknown and we model it with random processes. The filters use ideas from common seismic imaging techniques, such as normal move-out and semblance velocity estimation. These methods are based on the single scattering approximation, so it is surprising that the filters can annihilate the incoherent echoes produced by random media. The goal of the paper is to study theoretically and numerically this phenomenon.

Key words. array imaging, randomly layered media, filtering, velocity estimation.

1. Introduction. Sensor array imaging in heterogeneous media arises in important applications such as oil exploration, ground penetrating radar, ultrasonic nondestructive evaluation, etc. Multiple scattering by inhomogeneities in such media impedes the imaging process, because it creates echoes with long and noisy time traces at the array of sensors. The challenge is to extract efficiently the coherent information embedded in the noisy traces and image with it, without knowing the fluctuations in the medium.

In this paper we consider imaging with acoustic waves compactly supported objects buried deep in a strongly backscattering layered medium, occupying the half space $z < 0$, as illustrated in Figure 1.1. The data are collected with an array of sensors lying on the surface $z = 0$, in the set

$$\mathcal{A} = \left\{ \vec{\mathbf{x}} = (\mathbf{x}, 0), \quad \mathbf{x} \in \mathbb{R}^2, \quad |\mathbf{x}| \leq \frac{a}{2} \right\}, \tag{1.1}$$

where a is the array aperture. The sensor at $\vec{\mathbf{x}}_s \in \mathcal{A}$ is a source which probes the medium by emitting a short pulse and the receivers at $\vec{\mathbf{x}}_r \in \mathcal{A}$ record the resulting echoes. The recordings are time traces of the acoustic pressure field $P(t, \vec{\mathbf{x}}_r)$, for time t in a recording window (t_1, t_2).

The medium has sound speed $v(z)$ with smooth (or piecewise smooth) part denoted by $c(z)$ and a rough part that scatters. This rough part consists of fine layering and it may have in addition strong scattering interfaces caused by large jumps in $v(z)$ (see Figure 1.1). By fine layering we mean that $v(z)$ fluctuates rapidly, on a length scale ℓ that is small in comparison with the central wavelength λ_o of the signal emitted by the source at $\vec{\mathbf{x}}_s$. The fluctuations are strong, of order one. The object that we wish to image is at depth $-L$ and we say that it is buried deep in the medium because

$$\ell \ll \lambda_o \ll L. \tag{1.2}$$

The layered medium is unknown in practice and we cannot estimate it in detail from the array data. At best, we can determine the smooth part $c(z)$ and the depths of the strong scattering interfaces, if they exist. The sub-wavelength fluctuations of the sound speed cannot be estimated and we model the uncertainty about them with random processes. Wave propagation in randomly layered media under the assumption

†Computational and Applied Mathematics, Rice University, MS 134, Houston, TX 77005-1892. (borcea@caam.rice.edu and fcueto@caam.rice.edu)

‡Mathematics, Stanford University, Stanford CA 94305. (papanico@math.stanford.edu)

§Applied Mathematics, University of Crete, GR-71409 Heraklion, Greece (tsogka@tem.uoc.gr)

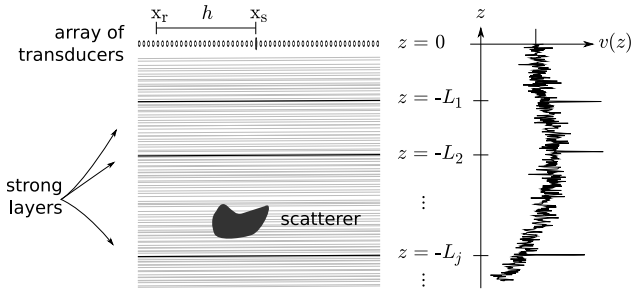

FIG. 1.1. *A compactly supported scatterer is buried in a layered medium with sound speed $v(z)$. The array of transducers lies on the top surface $z = 0$ and it consists of sources and receivers at locations denoted by $\mathbf{x}_s$ and $\mathbf{x}_r$. The medium is finely layered and it may have some strong scattering interfaces at depths $-L_j$, for $j = 1, 2, \ldots M$.*

(1.2) of separation of scales is studied in detail in [21, 1, 15, 24]. The coherent part of the wave field, which is needed in imaging, is described by the O'Doherty Anstey (ODA) theory [21, 1, 22, 15, 24]. ODA says that if we observe $P(t, \vec{\mathbf{x}}_r)$ in a time window of width similar to that of the source pulse, centered at travel times computed with speed $c(z)$, between the array and the coherent scattering structures*, we have deterministic signals except for small random time shifts. However, the coherent energy decays as the waves go deeper in the medium, due to scattering by the random layers that transfers energy to the incoherent field observed at the array as long tailed, noisy echoes (coda). The decay of coherent energy is exponential with depth and it occurs on a length scale L_{loc} called the localization length, which depends on the frequency and the direction of propagation of the waves. The loss of coherence is faster at the higher frequencies in the bandwidth and we observe a pulse broadening of the coherent arrivals [21, 1, 22, 15, 24].

Objects buried at shallow depths $L \ll L_{loc}$ produce strong coherent echoes at the array, and they can be imaged with Kirchhoff migration and its variants used in radar [10, 17], seismic imaging [4, 13, 6] etc., as noted in [9, 7]. However, Kirchhoff migration does not work for scattering objects that are buried deep in the medium, because of the low signal to noise ratio (SNR) at the array: The echoes from the layers (the "noise") typically overwhelm the coherent arrivals (the "signal") from the objects that we seek, and they must be filtered from the data before imaging.

The annihilation of the echoes produced by layered structures, for emphasis of the response of small diffractors buried in them, has been considered before in the geophysics literature [14, 19]. Examples are the plane-wave destruction filters [14, 19, 20] that remove from the data a sequence of plane-like waves arriving from different directions. The filters studied in this paper are based on the fact that the echoes from compactly supported scatterers and the echoes from the layers have a different signature in the time and source-receiver offset space. The main ideas come from well known techniques in seismic imaging such as normal move-out, gather flattening [14] and semblance velocity estimation [12, 25]. All these methods are based on the single scattering approximation and so are the filters, which are designed to remove the *primary echoes* that have been reflected *once* at some layer in the medium. However, numerical simulations reveal that the filters are surprisingly efficient at annihilating the echoes produced by randomly layered media,

*We call coherent scattering structures the strong interfaces and the compactly supported object that we wish to find. These structures create coherent echoes that are transmitted through the random medium as described by the ODA theory.

where multiple reflections dominate. The main goal of this paper is to study theoretically and numerically this phenomenon.

The annihilation of coherent echoes produced by strong scattering interfaces embedded in randomly layered media has been studied in [8], using the ODA theory. In this paper we analyze the annihilation of the incoherent arrivals caused by backscattering in the random medium. The efficiency of the annihilator filters depends on the average speed $c(z)$, which enters explicitly in their mathematical formulation. If we do not know $c(z)$, we can define the filters at a trial speed $\tilde{c}(z)$. It turns out that the annihilators work only when the trial speed is close to the true one, and this is why we can use them to estimate $c(z)$.

The paper is organized as follows: We begin in section 2 with the mathematical model for the pressure field recorded at the array. We define and analyze the layer annihilator filters in section 3. The numerical results are in section 4. We end with a summary and conclusions in section 5.

2. Formulation of the problem. To write the mathematical model of the data recorded at the receiver locations $\vec{\mathbf{x}}_r$ in the array $\mathcal{A}$, we begin with the acoustic wave equation. Then, we introduce the scaling and the random model of the fluctuations of the sound speed. The pressure field $P(t, \vec{\mathbf{x}}_r)$ at the array is modeled as a superposition of up going plane waves, with amplitudes determined by the reflection and transmission coefficients of the random medium. The statistics of these coefficients is given in [1, 21], and we recall here the relevant results to our analysis. They are moment formulae that we use in section 3 to calculate the intensity of the echoes before and after applying the annihilator filters.

2.1. The wave equation in the randomly layered medium. The pressure $P(t, \vec{\mathbf{x}})$ and velocity $\vec{\mathbf{u}}(t, \vec{\mathbf{x}})$ solve the acoustic wave equations

$$\begin{aligned} \rho \frac{\partial \vec{\mathbf{u}}}{\partial t}(t, \vec{\mathbf{x}}) + \nabla P(t, \vec{\mathbf{x}}) &= \vec{\mathbf{F}}(t, \vec{\mathbf{x}}), \\ \frac{1}{V^2(\vec{\mathbf{x}})} \frac{\partial P}{\partial t}(t, \vec{\mathbf{x}}) + \rho \nabla \cdot \vec{\mathbf{u}}(t, \vec{\mathbf{x}}) &= 0, \quad \vec{\mathbf{x}} = (\mathbf{x}, z) \in \mathbb{R}^d, \quad t > 0, \\ \vec{\mathbf{u}}(t, \vec{\mathbf{x}}) = \vec{\mathbf{0}}, \quad P(t, \vec{\mathbf{x}}) &= 0, \quad \text{for } t < 0, \end{aligned} \tag{2.1}$$

in the layered medium with sound speed $v(z)$ and density ρ taken constant for simplicity. The dimension of the space in (2.1) is $d \geq 2$, and we introduce the coordinate system $\vec{\mathbf{x}} = (\mathbf{x}, z)$ with the z axis orthogonal to the layers. To fix ideas, we take $d = 3$ in the analysis, but the results extend trivially to two dimensions.

We assume a fixed, point-like source at $\vec{\mathbf{x}}_s$, which emits a short pulse $\vec{\mathbf{F}}(t, \vec{\mathbf{x}})$ at time $t = 0$. The receivers at $\vec{\mathbf{x}}_r \in \mathcal{A}$ record the echoes $P(\vec{\mathbf{x}}_r, t)$, for times $t > 0$. The echoes are due to backscattering in the layered medium and to scattering at the object that we wish to image. This object has reflectivity $\nu(\vec{\mathbf{x}})$, supported in a compact set $\mathcal{S}$ of small diameter with respect to the array aperture a, and with center at depth $-L$.

The speed $V(\vec{\mathbf{x}})$ in (2.1) satisfies

$$\frac{1}{V^2(\vec{\mathbf{x}})} = \frac{1}{v^2(z)} + \nu(\vec{\mathbf{x}}), \tag{2.2}$$

for points $\vec{\mathbf{x}}$ in the half space $z < 0$ and $V(\vec{\mathbf{x}}) = c_o$ for $z \geq 0$. The speed $v(z)$ in the layered medium has a smooth part $c(z)$, which determines the kinematics of the waves (i.e., travel times) and a rough part that scatters. The rough part may consist of strong scattering interfaces due to large jumps of $v(z)$ and of fine

layering at scale $\ell \ll \lambda_o$. The annihilation of the coherent echoes produced by strong interfaces is studied in [8]. In this paper we are concerned only with the annihilation of the waves backscattered by the finely layered medium, so we assume that no strong interfaces exist.

The layered medium is unknown in practice and we cannot estimate it in detail from the array data. We can determine the smooth part $c(z)$ of the sound speed [12, 25] but not the sub-wavelength fluctuations, which we model with a random process as follows

$$\frac{1}{v^2(z)} = \frac{1}{c^2(z)}\left[1 + \sigma\mu\left(\frac{z}{\ell}\right)\right], \quad z < 0. \tag{2.3}$$

Here μ is a dimensionless, zero-mean and statistically homogeneous random function of dimensionless argument, which lacks long range correlations. That is to say, the correlation function

$$\mathcal{C}(z) = E\left\{\mu(0)\mu(z)\right\} \tag{2.4}$$

decays sufficiently fast at infinity to be integrable over the real line. The process is normalized by

$$\mathcal{C}(0) = 1, \quad \int_{-\infty}^{\infty} \mathcal{C}(z)dz = 1, \tag{2.5}$$

so that

$$\int_{-\infty}^{\infty} E\left\{\mu(0)\mu\left(\frac{z}{\ell}\right)\right\} dz = \ell, \tag{2.6}$$

with ℓ being the correlation length of the fluctuations. The intensity of the fluctuations is

$$E\left\{\left[\sigma\mu\left(\frac{z}{\ell}\right)\right]^2\right\} = \sigma^2, \tag{2.7}$$

and we control it by adjusting the dimensionless parameter $\sigma \leq O(1)$. We cannot have $\sigma \gg 1$ because of the bound constraint

$$\sigma|\mu(z)| < 1 \quad \text{for all } z < 0, \tag{2.8}$$

which ensures the positivity of the right hand side in (2.3).

At $z = 0$ we take the matching condition $c(0) = c_o$, to avoid a reverberating interface at the surface of the array, and to focus our study on the incoherent wave field backscattered by the random medium.

2.2. Scaling. In applications such as exploration geophysics [26] the waves penetrate to depths $L = 5 - 10$km that are much larger than the central wavelength $\lambda_o \sim 100$m of the probing pulses. The medium fluctuates on a much shorter scale $\ell = 2 - 3$m, and the fluctuations can be strong, of order one. The analysis in this paper is in such a regime, modeled with the assumption of separation of scales

$$\frac{\lambda_o}{L} \ll 1, \quad \frac{\ell}{\lambda_o} \ll 1, \quad \sigma = O(1). \tag{2.9}$$

Let L be the reference length scale and introduce a dimensionless parameter $\epsilon \ll 1$ by scaling the width of the pulse emitted from $\vec{\mathbf{x}}_s$ with the reference travel time L/c_o. We take

$$\vec{\mathbf{F}}(t, \vec{\mathbf{x}}) = \delta(\vec{\mathbf{x}} - \vec{\mathbf{x}}_s)\begin{pmatrix} \mathbf{F}^\epsilon(t) \\ f^\epsilon(t) \end{pmatrix} = \delta(\vec{\mathbf{x}} - \vec{\mathbf{x}}_s)\sqrt{\epsilon}\begin{pmatrix} \mathbf{F}(t/\epsilon) \\ f(t/\epsilon) \end{pmatrix}, \tag{2.10}$$

and we scale the amplitude of the source by $\sqrt{\epsilon}$ to get $O(1)$ incoherent echoes at the array, as shown in section 3. The source has arbitrary directivity and $f(t)$, $\mathbf{F}(t)$ are base-band signals with central frequency ω_o and bandwidth B. In the Fourier domain we have

$$\hat{\mathbf{F}}^\epsilon\left(\frac{\omega}{\epsilon}\right) = \int \mathbf{F}^\epsilon(t) e^{i\frac{\omega}{\epsilon}t}\, dt = \epsilon^{\frac{3}{2}} \int \mathbf{F}\left(\frac{t}{\epsilon}\right) e^{i\omega\frac{t}{\epsilon}}\, \frac{dt}{\epsilon} = \epsilon^{\frac{3}{2}} \hat{\mathbf{F}}(\omega),$$
$$\hat{f}^\epsilon\left(\frac{\omega}{\epsilon}\right) = \epsilon^{\frac{3}{2}} \hat{f}(\omega), \tag{2.11}$$

which means that the source (2.10) is supported on the high frequencies

$$\omega^\epsilon = \frac{\omega}{\epsilon} \in \left[\frac{\omega_o}{\epsilon} - \frac{B}{2\epsilon}, \frac{\omega_o}{\epsilon} + \frac{B}{2\epsilon}\right] \bigcup \left[-\frac{\omega_o}{\epsilon} - \frac{B}{2\epsilon}, -\frac{\omega_o}{\epsilon} + \frac{B}{2\epsilon}\right].$$

This is consistent with (2.9), and we change from now on the notation of the central wavelength to λ_o^ϵ, to emphasize that it is an $O(\epsilon)$ length scale,

$$\frac{\lambda_o^\epsilon}{L} = O(\epsilon) \ll 1. \tag{2.12}$$

We also rename the correlation length ℓ^ϵ, and we assume it is $O(\epsilon^2)$, while keeping the strength of the fluctuations $\sigma = O(1)$. Explicitly, we write

$$\int_{-\infty}^{\infty} E\left\{\sigma\mu(0)\sigma\mu\left(\frac{z}{\ell^\epsilon}\right)\right\} dz = \ell^\epsilon \sigma^2 = \epsilon^2 l, \tag{2.13}$$

with $l = \sigma^2 \ell^\epsilon/\epsilon^2$ the $O(1)$ rescaled correlation length.

Our model of separation of scales (2.9) is

$$\frac{\ell^\epsilon}{\lambda_o^\epsilon} \sim \frac{\lambda_o^\epsilon}{L} \sim \epsilon \ll 1, \quad \sigma \sim 1, \tag{2.14}$$

and we let the remaining length scale a, the array aperture, be much larger than λ_o^ϵ and independent of ϵ. The filters need such an aperture to make a robust differentiation between the layer echoes and the coherent arrivals from the compact scatterers that we wish to image. Imaging and velocity estimation, with or without layer filtering, require an aperture $a \gg \lambda_o^\epsilon$ [6, 13, 4, 12, 8].

Note that (2.14) is a high frequency regime with respect to the large scale variations in the medium, but it is low frequency with respect to the small scale ℓ^ϵ. Because $\lambda_o^\epsilon \gg \ell^\epsilon$, the waves do not interact strongly with the layers, although they are strong ($\sigma \sim 1$), and the random effects average out over distances of order λ_o^ϵ. However, the backscattering builds up over the long distances of propagation $L \gg \lambda_o^\epsilon$ considered in (2.14), and it becomes a significant component of the data recorded at the array.

There are other scaling regimes that give significant backscattering and that can be analyzed [1, 21]. For example, the theory in this paper extends almost identically to the *weakly heterogeneous* regime with $\sigma \ll 1$, $L \gg \lambda_o^\epsilon$, and correlation length similar to λ_o^ϵ. The difference is that in the weakly heterogeneous regime the waves sample more efficiently the small scales, and the asymptotic results depend on the specific autocorrelation function of the random fluctuations [21]. In our regime the waves cannot see the small scales in detail, because $\lambda_o^\epsilon \gg \ell^\epsilon$, and in the limit $\epsilon \to 0$ the fluctuations take the canonical form of *white noise*, independent of the detailed structure of the random function μ.

2.3. The scattered field. The pressure field $P(t, \vec{\mathbf{x}}_r)$ recorded at the array consists of two parts: The direct arrival from the source at $\vec{\mathbf{x}}_s$, and the scattered field $p(t, \vec{\mathbf{x}}_r)$. The direct arrival carries no information about the medium and it can be removed by tapering the data for $t \leq |\vec{\mathbf{x}}_r - \vec{\mathbf{x}}_s|/c_o$.

Let us call $\mathcal{L}_t$ the maximum depth of penetration of the waves, up to time t, and define

$$\tau_c^{\mathcal{S}} = \min_{\vec{\mathbf{y}} \in \mathcal{S},\ \vec{\mathbf{x}}_r \in \mathcal{A}} \tau_c(\vec{\mathbf{x}}_s, \vec{\mathbf{y}}, \vec{\mathbf{x}}_r), \tag{2.15}$$

using the travel time $\tau_c(\vec{\mathbf{x}}_s, \vec{\mathbf{y}}, \vec{\mathbf{x}}_r)$ computed at speed[†] $c(z)$, from $\vec{\mathbf{x}}_s \in \mathcal{A}$ to $\vec{\mathbf{y}} \in \mathcal{S}$ and then back to the array, at receiver location $\vec{\mathbf{x}}_r \in \mathcal{A}$. The scattered field $p(t, \vec{\mathbf{x}}_r)$ observed at times $t < \tau_c^{\mathcal{S}}$ consists of the echoes from the random medium above depth $-\mathcal{L}_t > -L$, and it is given by the solution of the wave equation

$$\begin{aligned} \rho \frac{\partial \vec{\mathbf{u}}}{\partial t}(t, \vec{\mathbf{x}}) + \nabla P(t, \vec{\mathbf{x}}) &= \vec{\mathbf{F}}(t, \vec{\mathbf{x}}), \\ \frac{1}{v^2(z)} \frac{\partial P}{\partial t}(t, \vec{\mathbf{x}}) + \rho \nabla \cdot \vec{\mathbf{u}}(t, \vec{\mathbf{x}}) &= 0, \quad \vec{\mathbf{x}} = (\mathbf{x}, z) \in \mathbb{R}^3, \quad 0 < t < \tau_c^{\mathcal{S}}, \\ \vec{\mathbf{u}}(t, \vec{\mathbf{x}}) = \vec{\mathbf{0}}, \quad P(t, \vec{\mathbf{x}}) &= 0, \quad \text{for } t < 0, \end{aligned} \tag{2.16}$$

after removing the direct arrival.

When $t > \tau_c^{\mathcal{S}}$, the waves have reached the object in $\mathcal{S}$ and the scattered field contains the echoes $p^{\mathcal{S}}(t, \vec{\mathbf{x}}_r)$ from the reflectivity $\nu(\vec{\mathbf{x}})$. We model these echoes with the Born approximation

$$p^{\mathcal{S}}(t, \vec{\mathbf{x}}_r) \approx -\int_{\mathcal{S}} d\vec{\mathbf{y}}\, \nu(\vec{\mathbf{y}})\, \frac{\partial^2 P^i(t, \vec{\mathbf{y}})}{\partial t^2} \star_t G(t, \vec{\mathbf{x}}_r, \vec{\mathbf{y}}), \tag{2.17}$$

where $\star_t$ denotes time convolution, G is the causal Green's function of the wave equation in the layered medium, and $P^i(t, \vec{\mathbf{y}})$ is the "incident" pressure field transmitted through the random medium, from $\vec{\mathbf{x}}_s$ to $\vec{\mathbf{y}} \in \mathcal{S}$. It satisfies equation (2.16), for all times $t > 0$.

2.3.1. The up and down going plane wave decomposition. It is convenient to analyze the backscattered and transmitted fields in the phase space, by taking the Fourier transform in (2.16) over t and the cross-range variable $\mathbf{x} \in \mathbb{R}^2$. We have

$$\begin{aligned} \hat{P}\left(\frac{\omega}{\epsilon}, \mathbf{K}, z\right) &= \int dt \int d\mathbf{x}\, P(t, \mathbf{x}, z) e^{i\frac{\omega}{\epsilon}(t - \mathbf{K}\cdot\mathbf{x})}, \\ (\hat{\mathbf{u}}, \hat{u})\left(\frac{\omega}{\epsilon}, \mathbf{K}, z\right) &= \int dt \int d\mathbf{x}\, \vec{\mathbf{u}}(t, \mathbf{x}, z) e^{i\frac{\omega}{\epsilon}(t - \mathbf{K}\cdot\mathbf{x})}, \quad \vec{\mathbf{u}} = (\mathbf{u}, u), \end{aligned} \tag{2.18}$$

where we scale the frequency by $1/\epsilon$, as explained in section 2.2 and we let the dual variable to $\mathbf{x}$ in the plane wave decomposition be the horizontal slowness vector $\mathbf{K}$. This vector has units of time over length and its magnitude $K = |\mathbf{K}|$ scales as $1/c_o$.

Eliminating $\hat{\mathbf{u}}$ from the equations (2.16), after the Fourier transform, we get a one dimensional problem for oblique plane waves in the random medium,

$$\begin{aligned} \frac{i\omega}{\epsilon}\left[K^2 - \frac{1}{v^2(z)}\right]\hat{P} + \rho \frac{\partial \hat{u}}{\partial z} &= 0, \\ -\frac{i\omega}{\epsilon}\rho \hat{u} + \frac{\partial \hat{P}}{\partial z} &= 0, \quad z < 0. \end{aligned} \tag{2.19}$$

[†]It is a consequence of the ODA theory [1, 15, 24] that we can use travel times computed with speed $c(z)$ to decide if the waves have reached the scatterer in $\mathcal{S}$ or not. ODA says that the first echoes scattered at $\vec{\mathbf{y}} \in \mathcal{S}$ arrive at times $\tau_c(\vec{\mathbf{x}}_s, \vec{\mathbf{y}}, \vec{\mathbf{x}}_r) + O(\epsilon)$.

The source excitation (2.10) translates into jump conditions at $z = 0$,

$$\hat{P}\left(\frac{\omega}{\epsilon}, \mathbf{K}, 0^+\right) - \hat{P}\left(\frac{\omega}{\epsilon}, \mathbf{K}, 0^-\right) = \epsilon^{\frac{3}{2}} \hat{f}(\omega) e^{-i\frac{\omega}{\epsilon}\mathbf{K}\cdot\mathbf{x}_s},$$
$$\hat{u}\left(\frac{\omega}{\epsilon}, \mathbf{K}, 0^+\right) - \hat{u}\left(\frac{\omega}{\epsilon}, \mathbf{K}, 0^-\right) = \frac{\epsilon^{\frac{3}{2}} \mathbf{K}\cdot\hat{\mathbf{F}}(\omega)}{\rho} e^{-i\frac{\omega}{\epsilon}\mathbf{K}\cdot\mathbf{x}_s}. \tag{2.20}$$

To model the up going pressure field recorded at the array and the down going field impinging on $\mathcal{S}$, we decompose further $\hat{P}$ and $\hat{u}$ into up and down going waves. Following [21, 1], we write

$$\hat{P}\left(\frac{\omega}{\epsilon}, \mathbf{K}, z\right) = \frac{\sqrt{\rho c(K,z)}}{2}\left[\hat{\alpha}^\epsilon(\omega, \mathbf{K}, z) e^{i\frac{\omega}{\epsilon}\tau(K,z)} - \hat{\beta}^\epsilon(\omega, \mathbf{K}, z) e^{-i\frac{\omega}{\epsilon}\tau(K,z)}\right],$$
$$\hat{u}\left(\frac{\omega}{\epsilon}, \mathbf{K}, z\right) = \frac{1}{2\sqrt{\rho c(K,z)}}\left[\hat{\alpha}^\epsilon(\omega, \mathbf{K}, z) e^{i\frac{\omega}{\epsilon}\tau(K,z)} + \hat{\beta}^\epsilon(\omega, \mathbf{K}, z) e^{-i\frac{\omega}{\epsilon}\tau(K,z)}\right], \tag{2.21}$$

where α^ϵ and β^ϵ are random variables quantifying the amplitude of the up and down going plane waves, at frequency ω, depth z and slowness $\mathbf{K}$. The remaining terms in (2.21) are the smooth vertical speed

$$c(K, z) = \frac{c(z)}{\sqrt{1 - c^2(z)K^2}}, \tag{2.22}$$

and the travel time to depth z [‡]

$$\tau(K, z) = \int_0^z \frac{dz'}{c(K, z')}. \tag{2.23}$$

The "amplitudes" α^ϵ and β^ϵ satisfy a coupled system of stochastic ordinary differential equations for $z < 0$, obtained by substituting (2.21) in (2.19). These equations can be found in [21, 1], but we do not use them directly in the analysis. We only need the initial conditions at the array surface,

$$\alpha^\epsilon(\omega, \mathbf{K}, 0^+) = \alpha^\epsilon(\omega, \mathbf{K}, 0^-) + \frac{\epsilon^{\frac{3}{2}} e^{-i\frac{\omega}{\epsilon}\mathbf{K}\cdot\mathbf{x}_s}}{\sqrt{\rho c(K,0)}}\left[\hat{f}(\omega) + c(K,0)\mathbf{K}\cdot\hat{\mathbf{F}}(\omega)\right],$$
$$\beta^\epsilon(\omega, \mathbf{K}, 0^-) = \frac{\epsilon^{\frac{3}{2}} e^{-i\frac{\omega}{\epsilon}\mathbf{K}\cdot\mathbf{x}_s}}{\sqrt{\rho c(K,0)}}\hat{\varphi}(\omega, \mathbf{K}), \tag{2.24}$$

derived from (2.20)-(2.21) and the identity

$$\beta^\epsilon(\omega, \mathbf{K}, 0^+) = 0, \tag{2.25}$$

which says that there are no downgoing waves above the source, in the homogeneous half space $z > 0$. Thus, $\beta^\epsilon(\omega, \mathbf{K}, 0^-)$ is the down going field emitted by the source at $\vec{\mathbf{x}}_s$, and

$$\hat{\varphi}(\omega, \mathbf{K}) = \hat{f}(\omega) - c(K,0)\mathbf{K}\cdot\hat{\mathbf{F}}(\omega) \tag{2.26}$$

is the pulse shape. The upgoing $\alpha^\epsilon(\omega, \mathbf{K}, 0^+)$ consists of two parts: The direct arrival that has no information about the medium, and the reflected $\alpha^\epsilon(\omega, \mathbf{K}, 0^-)$ that defines the backscattered field at the array.

The incident field $P^i(t, \vec{\mathbf{y}})$ at point $\vec{\mathbf{y}} = (\mathbf{y}, \eta - L) \in \mathcal{S}$ is determined by the *transmitted* $\beta^\epsilon(\omega, \mathbf{K}, \eta - L)$, and $G(t, \vec{\mathbf{y}}, \vec{\mathbf{x}}_r)$ follows similarly, by reciprocity.

[‡]Note that $\tau(K, z)$ is the travel time for the one dimensional problem of oblique plane waves propagating at vertical speed $c(K, z)$. It is not the same as the travel time of three dimensional waves, denoted by τ_c in equation (2.15).

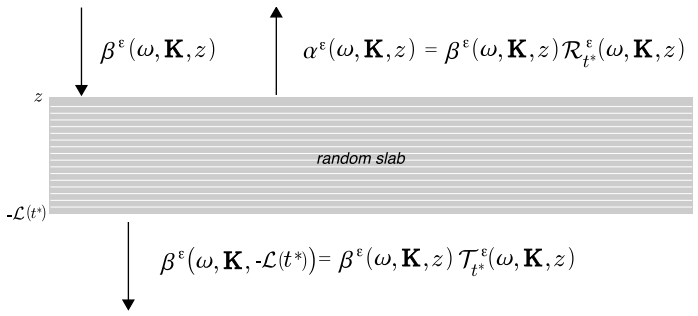

FIG. 2.1. *Schematic of transmission and reflection by a random slab in the depth interval* $(-\mathcal{L}_{t^\star}, z)$.

2.3.2. Reflection and transmission coefficients. When we observe $p(t,\vec{\mathbf{x}}_r)$ at times $t \le t^\star < \tau_c^{\mathcal{S}}$, we cannot get echoes from depths larger than $-\mathcal{L}_{t^\star}$, so we may set

$$\alpha^\epsilon(\omega,\mathbf{K},-\mathcal{L}_{t^\star}) = 0. \tag{2.27}$$

Now consider an arbitrary $z \in (-\mathcal{L}_{t^\star}, 0)$, as illustrated in Figure 2.1, and define the reflection and transmission coefficients $\mathcal{R}^\epsilon_{t^\star}$ and $\mathcal{T}^\epsilon_{t^\star}$ of the random medium contained in the depth interval $(-\mathcal{L}_{t^\star}, z)$,

$$\mathcal{R}^\epsilon_{t^\star}(\omega,K,z) = \frac{\alpha^\epsilon(\omega,\mathbf{K},z)}{\beta^\epsilon(\omega,\mathbf{K},z)} \quad \text{and} \quad \mathcal{T}^\epsilon_{t^\star}(\omega,K,z) = \frac{\beta^\epsilon(\omega,\mathbf{K},-\mathcal{L}_{t^\star})}{\beta^\epsilon(\omega,\mathbf{K},z)}. \tag{2.28}$$

These coefficients are random functions of ω, $K = |\mathbf{K}|$ and z, they satisfy the energy conservation identity[§]

$$|\mathcal{R}^\epsilon_{t^\star}(\omega,K,z)|^2 + |\mathcal{T}^\epsilon_{t^\star}(\omega,K,z)|^2 = 1, \tag{2.29}$$

and their statistical distribution is understood in the limit $\epsilon \to 0$. We quote in section 2.4, from [21, 1], the relevant facts to our analysis.

2.3.3. The integral representation of the scattered field. The mathematical model of the backscattered field follows from (2.18), (2.21), (2.24) and (2.28)

$$p(t,\vec{\mathbf{x}}_r) = \frac{\epsilon^{\frac{3}{2}}}{2(2\pi)^3}\int\frac{d\omega}{\epsilon}\int d\mathbf{K}\left(\frac{\omega}{\epsilon}\right)^2\hat{\varphi}(\omega,\mathbf{K})\,\mathcal{R}^\epsilon_{t^\star}(\omega,K,0)e^{-i\frac{\omega}{\epsilon}t + i\frac{\omega}{\epsilon}\mathbf{K}\cdot(\mathbf{x}_r-\mathbf{x}_s)}, \tag{2.30}$$

for observation times $t \le t^\star < \tau_c^{\mathcal{S}}$.

The model of the incident field $P^i(t,\vec{\mathbf{y}})$ at $\vec{\mathbf{y}} = (\mathbf{y}, \eta - L) \in \mathcal{S}$ is determined by the ballistic, down going part

$$\beta^\epsilon(\omega,K,\eta-L) = \beta^\epsilon(\omega,\mathbf{K},0^-)\mathcal{T}^\epsilon_{t^\star}(\omega,K,0), \tag{2.31}$$

for $t^\star$ satisfying $-\mathcal{L}_{t^\star} = \eta - L$, and by additional, weaker reverberations from the random medium. We have

$$P^i(t,\vec{\mathbf{y}}) \approx -\frac{\epsilon^{\frac{3}{2}}}{2(2\pi)^3}\int\frac{d\omega}{\epsilon}\int d\mathbf{K}\left(\frac{\omega}{\epsilon}\right)^2\hat{\varphi}(\omega,\mathbf{K})\,\mathcal{T}^\epsilon_{t^\star}(\omega,K,0)e^{-i\frac{\omega}{\epsilon}(t+\tau(K,\eta-L))+i\frac{\omega}{\epsilon}\mathbf{K}\cdot(\mathbf{y}-\mathbf{x}_s)} + \ldots, \tag{2.32}$$

where we denote by "..." the reverberations. The Green's function $G(t,\vec{\mathbf{y}},\vec{\mathbf{x}}_r)$ is similar, by reciprocity, and $p^{\mathcal{S}}(t,\vec{\mathbf{x}}_r)$ is determined by the time convolution of $\frac{\partial^2 P^i}{\partial t^2}$ with the Green's function, according to the Born formula (2.17).

[§]This identity follows by direct calculation from (2.19), (2.21) and (2.28), as shown in [21, Section 17.2].

2.4. Asymptotics of the reflection and transmission coefficients. Definition (2.28) of $\mathcal{R}^\epsilon_{t^\star}(\omega, K, z)$ and (2.19), (2.21) give a Ricatti equation for the reflection coefficients [21, 1],

$$\frac{\partial}{\partial z}\mathcal{R}^\epsilon_{t^\star}(\omega,K,z) = -\frac{-i\omega\mu^\epsilon(z)}{2c(z)\sqrt{1-c^2(z)K^2}}\left\{e^{-2i\frac{\omega}{\epsilon}\tau(K,z)} - 2\mathcal{R}^\epsilon_{t^\star}(\omega,K,z) + e^{2i\frac{\omega}{\epsilon}\tau(K,z)}\left[\mathcal{R}^\epsilon_{t^\star}(\omega,K,z)\right]^2\right\}$$
$$+\frac{\partial}{\partial z}\ln\sqrt{c(K,z)}\left\{e^{-2i\frac{\omega}{\epsilon}\tau(K,z)} - e^{2i\frac{\omega}{\epsilon}\tau(K,z)}\left[\mathcal{R}^\epsilon_{t^\star}(\omega,K,z)\right]^2\right\}, \quad z > -\mathcal{L}_{t^\star}, \tag{2.33}$$

with initial condition

$$\mathcal{R}^\epsilon_{t^\star}(\omega,K,-\mathcal{L}_{t^\star}) = 0, \tag{2.34}$$

derived from (2.27), and with the random driving function

$$\mu^\epsilon(z) = \frac{\sigma}{\epsilon}\mu\left(\frac{z}{(\epsilon/\sigma)^2 l}\right). \tag{2.35}$$

The second term in the right hand side of (2.33) averages out in the limit $\epsilon \to 0$, because of the $O(1/\epsilon)$ phases [21, Theorem 6.4], so we can neglect it. For μ^ϵ we have by the central limit theorem that as $\epsilon \to 0$,

$$\int_{-\mathcal{L}_{t^\star}}^{z} \mu^\epsilon(z')dz' \to \sqrt{l}\, W(z), \tag{2.36}$$

where $W(z)$ is standard Brownian motion and the convergence is weak, in distribution. Thus, the random fluctuations in the medium take the canonical form of *white noise* as $\epsilon \to 0$, and we can calculate all the limit moments of $\mathcal{R}^\epsilon_{t^\star}$ using the white noise (diffusion) limit theorems in [5, 23] and [21, Section 6.5]. Our analysis requires the first and second moments of $\mathcal{R}^\epsilon_{t^\star}(\omega, K, 0)$, which we quote directly from [21, 1]:

LEMMA 2.1. *The reflection coefficients $\mathcal{R}^\epsilon_{t^\star}(\omega, K, z)$ have mean zero and they decorrelate rapidly over ω and K. As $\epsilon \to 0$, we have the following limits of the second moments of $\mathcal{R}^\epsilon_{t^\star}$, evaluated at $z = 0$:*

$$E\left\{\mathcal{R}^\epsilon_{t^\star}(\omega,K,0)\overline{\mathcal{R}^\epsilon_{t^\star}(\omega',K',0)}\right\} \to 0, \quad \text{if } \frac{|\omega-\omega'|}{\omega_o} > O(\epsilon) \text{ or } c_o|K-K'| > O(\epsilon), \tag{2.37}$$

and

$$E\left\{\mathcal{R}^\epsilon_{t^\star}\left(\omega+\frac{\epsilon\tilde{\omega}}{2}, K+\frac{\epsilon\tilde{K}}{2}, 0\right)\overline{\mathcal{R}^\epsilon_{t^\star}\left(\omega-\frac{\epsilon\tilde{\omega}}{2}, K-\frac{\epsilon\tilde{K}}{2}, 0\right)}\right\} \to \int_{-\infty}^{\infty}ds\int_{-\infty}^{\infty}d\chi\, W_1(\omega,K,s,\chi,0)$$
$$exp\left[i\tilde{\omega}(s-K\chi) - i\omega\tilde{K}\chi\right], \tag{2.38}$$

where the bar denotes complex conjugate. The limit in (2.38) depends on the solution of the infinite system of transport equations

$$\frac{\partial W_N}{\partial z} + \frac{2N}{c(z)\sqrt{1-c^2(z)K^2}}\frac{\partial W_N}{\partial s} + \frac{2Nc(z)K}{\sqrt{1-c^2(z)K^2}}\frac{\partial W_N}{\partial \chi} = \frac{N^2}{L_{loc}}\left(W_{N+1} - 2W_N + W_{N-1}\right), \quad z > -\mathcal{L}_{t^\star},$$
$$W_N(\omega,K,s,\chi,z=-\mathcal{L}_{t^\star}) = \delta_{0,N}\delta(s)\delta(\chi), \quad N \in \mathbb{Z}, \quad N \geq 0. \tag{2.39}$$

The solutions $W_N(\omega, K, s, \chi, z)$ determine the $2N$-th order moments of $\mathcal{R}^\epsilon_{t^\star}(\omega, K, z)$, at nearby frequencies and slownesses. Because $\mathcal{R}^\epsilon_{t^\star}(\omega, K, -\mathcal{L}_{t^\star}) = 0$, we have the initial conditions $W_N(\omega, K, \sigma, \chi, -\mathcal{L}_{t^\star}) = 0$ for

$N \neq 0$, as denoted by the Kronecker delta symbol $\delta_{0,N}$ in (2.39). The right hand side in (2.39) depends on the localization length

$$L_{loc}(\omega, K, z) = \frac{4c^2(z)\left[1 - c^2(z)K^2\right]}{\omega^2 l}, \tag{2.40}$$

which is the length scale of exponential decay of the coherent part of the wavefield, as we discuss below.

The transmission coefficients $\mathcal{T}^{\epsilon}_{t^\star}(\omega, K, 0)$ carry the coherent part of the wave field and their moments are summarized in the next lemma, quoted from [21, 1].

LEMMA 2.2. *The multi frequency and slowness moments of the transmission coefficients $\mathcal{T}^{\epsilon}_{t^\star}(\omega, K, z)$ converge in the limit $\epsilon \to 0$ to the moments of the O'Doherty Anstey (ODA) kernel*

$$\mathcal{T}^{ODA}_{t^\star}(\omega, K, z) = exp\left\{-\frac{1}{2}\int_{-\mathcal{L}_{t^\star}}^{z} \frac{dz'}{L_{loc}(\omega, K, z')} + i\int_{-\mathcal{L}_{t^\star}}^{z} \frac{dW(z')}{\sqrt{L_{loc(\omega,K,z')}}}\right\}. \tag{2.41}$$

That is,

$$E\left\{\prod_{q\geq 1} \mathcal{T}^{\epsilon}_{t^\star}(\omega_q, K_q, z)\right\} \to E\left\{\prod_{q\geq 1} \mathcal{T}^{ODA}_{t^\star}(\omega_q, K_q, z)\right\} \quad for \ \ \epsilon \to 0. \tag{2.42}$$

2.5. The SNR at the array. We conclude easily from Lemma 2.1 and (2.30) that the expectation of the pressure field backscattered by the random medium is zero. This is why we call (2.30) the *incoherent* field recorded at the array. The coherent part is transmitted through the random medium from the array, to the scatterer in $\mathcal{S}$ and back to $\mathcal{A}$. It is embedded in the incoherent echoes and we wish to extract it efficiently for imaging $\mathcal{S}$. We calculate here the intensity of the coherent echoes and show that when $\mathcal{S}$ is buried deep in the medium, the data are dominated by the incoherent field. This is the regime where layer annihilator filters can make a dramatic difference for imaging, as shown in sections 3 and 4.

2.5.1. The amplitude of the coherent field. To assess the intensity of the coherent field, let us look in detail at $P^i(t, \vec{\mathbf{y}})$, the incident field at point $\vec{\mathbf{y}} = (\mathbf{y}, \eta - L) \in \mathcal{S}$. We have from (2.33) and Lemma 2.2 that all the moments of $P^i(t, \vec{\mathbf{y}})$ are approximately equal to the moments of the ODA field

$$P^{ODA}(t, \vec{\mathbf{y}}) = -\frac{\epsilon^{\frac{3}{2}}}{2(2\pi)^3}\int \frac{d\omega}{\epsilon}\int d\mathbf{K}\left(\frac{\omega}{\epsilon}\right)^2 \hat{\varphi}(\omega, \mathbf{K}) \exp\left\{-i\frac{\omega}{\epsilon}\left[t + \tau(K, \eta - L)\right] + i\frac{\omega}{\epsilon}\mathbf{K}\cdot(\mathbf{y} - \mathbf{x}_s)\right.$$
$$\left. -\frac{1}{2}\int_{-L+\eta}^{0} \frac{dz'}{L_{loc}(\omega, K, z')} + i\int_{-L+\eta}^{0} \frac{dW(z')}{\sqrt{L_{loc(\omega,K,z')}}}\right\}, \tag{2.43}$$

if the observation time t is near the arrival time $\tau_c(\vec{\mathbf{y}}, \vec{\mathbf{x}}_s)$ of (2.43). This arrival time can be obtained with the method of stationary phase, which says that the main contribution in (2.43) comes from the neighborhood of slowness $\mathbf{K}$, the unique solution of equation[¶]

$$\mathbf{y} - \mathbf{x}_s = \nabla_{\mathbf{K}}\tau(K, \eta - L) = \int_{\eta - L}^{0} dz' \frac{\mathbf{K}\, c(z')}{\sqrt{1 - c^2(z')K^2}}, \tag{2.44}$$

[¶]The solution is unique because $\mathbf{K}$ is in the direction of $\mathbf{y} - \mathbf{x}_s$ and, after taking norms in (2.44), the right hand side is monotonically increasing with K.

and it can be observed in an $O(\epsilon)$ time window centered at

$$\tau_c(\vec{\mathbf{x}}_s,\vec{\mathbf{y}}) = -\tau(K,\eta-L) + \mathbf{K}\cdot(\mathbf{y}-\mathbf{x}_s) = \int_{\eta-L}^{0} \frac{dz'}{c(z')\sqrt{1-c^2(z')K^2}}. \tag{2.45}$$

For example, in the homogeneous case $c(z) = c_o$, we get the slowness magnitude

$$K = \frac{\cos\theta(\vec{\mathbf{y}},\vec{\mathbf{x}}_s)}{c_o}, \quad \cos\theta(\vec{\mathbf{y}},\vec{\mathbf{x}}_s) = \frac{|\mathbf{y}-\mathbf{x}_s|}{|\vec{\mathbf{y}}-\vec{\mathbf{x}}_s|},$$

and the travel time is $\tau_{c_o}(\vec{\mathbf{x}}_s,\vec{\mathbf{y}}) = |\vec{\mathbf{y}}-\vec{\mathbf{x}}_s|/c_o$. The ODA field follows after straightforward calculations

$$P^{ODA}(t,\vec{\mathbf{y}}) \approx -\frac{\partial}{\partial z}\left\{ \frac{\left[\left(f^\epsilon + \frac{(\mathbf{y}-\mathbf{x}_s)}{(L-\eta)}\cdot\mathbf{F}^\epsilon\right)\star_t \mathcal{N}^{ODA}\right]\left(t-\tau_{c_o}(\vec{\mathbf{y}},\vec{\mathbf{x}}_s) - \epsilon\delta\tau^{ODA}_{c_o}(\vec{\mathbf{y}},\vec{\mathbf{x}}_s)\right)}{4\pi|\vec{\mathbf{y}}-\vec{\mathbf{x}}_s|}\right\}\Bigg|_{z=\eta-L} \tag{2.46}$$

and if we compare it with

$$P_o(t,\vec{\mathbf{y}}) \approx -\frac{\partial}{\partial z}\left\{ \frac{\left[f^\epsilon + \frac{(\mathbf{y}-\mathbf{x}_s)}{(L-\eta)}\cdot\mathbf{F}^\epsilon\right](t-\tau_{c_o}(\vec{\mathbf{y}},\vec{\mathbf{x}}_s))}{4\pi|\vec{\mathbf{y}}-\vec{\mathbf{x}}_s|}\right\}\Bigg|_{z=\eta-L\,,}$$

the pressure field in the homogeneous medium, we conclude that: The random medium modifies the pulse shape and the amplitude of the coherent arrivals, via the convolution with the Gaussian kernel

$$\begin{aligned}\mathcal{N}^{ODA}(t) &= \int \frac{d\omega}{2\pi}\exp\left\{-i\omega t - \frac{L-\eta}{2L_{loc}(\omega,K_{c_o},0)}\right\} \\ &= \frac{\sin\theta(\vec{\mathbf{y}},\vec{\mathbf{x}}_s)}{\sqrt{2\pi}\,t_{ps}(L-\eta)}\exp\left\{-\frac{t^2\sin^2\theta(\vec{\mathbf{y}},\vec{\mathbf{x}}_s)}{2t^2_{ps}(L-\eta)}\right\}, \quad \text{where } \; t_{ps}(L-\eta) = \sqrt{\frac{l(L-\eta)}{2c_o^2}},\end{aligned} \tag{2.47}$$

and the arrival time has a small random shift

$$\epsilon\delta\tau^{ODA}_{c_o}(\vec{\mathbf{y}},\vec{\mathbf{x}}_s) = \frac{\epsilon t_{ps}(L-\eta)}{\sin\theta(\vec{\mathbf{y}},\vec{\mathbf{x}}_s)}\frac{W(L-\eta)}{\sqrt{L-\eta}},$$

determined by the Brownian motion $W(L-\eta)$.

The rapid decorrelation properties of the reflection coefficients $\mathcal{R}^\epsilon_{t^\star}(\omega,K,0)$ given in Lemma 2.1 suggest that the intensity of the backscattered field is smaller, by a factor of ϵ, than the intensity of the coherent field modeled by ODA. This is true if the objects that we wish to image are at shallow depths, but not if L is large. Equations (2.46) and (2.47) show that when $L \sim L_{loc}$, we have a significant loss of coherence of the incident field impinging on $\mathcal{S}$, and therefore of the echoes $p^{\mathcal{S}}(t,\vec{\mathbf{x}}_r)$. Because of scattering in the random medium, most of the energy is transfered to the incoherent field which overwhelms the faint coherent echoes that are useful in imaging $\mathcal{S}$. That is to say, we have low SNR at the array.

3. Layer annihiliation. We begin this section with the calculation of the intensity of the incoherent, backscatered field $p(t,\vec{\mathbf{x}}_r)$. Then, we define the layer annihilator filters and we show that they improve the SNR at the array, by suppressing the incoherent echoes.

3.1. Intensity of the backscattered field. Since the source is fixed at $\vec{\mathbf{x}}_s$, we parametrize the data by the source receiver-offset, and we assume for convenience in the analysis that the separation between the receivers is small enough to allow us to view the array as a continuum aperture. We write

$$p(t,\vec{\mathbf{x}}) = D(t,\mathbf{h}), \quad \vec{\mathbf{x}} = \vec{\mathbf{x}}_s + (\mathbf{h},0) \in \mathcal{A}, \tag{3.1}$$

and we call $D(t,\mathbf{h})$ the data, because it is what we record at times t satisfying $|\mathbf{h}|/c_o < t \leq t^\star < \tau_c^{\mathcal{S}}$. Recall that $E\{D(t,\mathbf{h})\} = 0$ and define its intensity as the variance $E\left\{[D(t,\mathbf{h})]^2\right\}$. This is computed in [21, 1], but we rederive it here as a particular case of the crosscorrelation of $D(t,\mathbf{h})$, needed in section 3.3.

LEMMA 3.1. *Let* $\mathbf{h}$ *and* $\mathbf{h}'$ *be two source-receiver offsets and suppose that they are collinear and they point in the same direction. Let also* t *and* t' *be two observation times. We have*

$$E\left\{D(t,\mathbf{h})D(t',\mathbf{h}')\right\} \to 0, \quad \textit{as} \quad \epsilon \to 0, \tag{3.2}$$

if $|\mathbf{h}-\mathbf{h}'|/a > O(\epsilon)$, *(i.e.,* $|\mathbf{h}-\mathbf{h}'| \gg \lambda_o^\epsilon$*) and/or* $|t-t'|/t^\star > O(\epsilon)$. *For nearby offsets* $\mathbf{h}' = \mathbf{h} + \epsilon\boldsymbol{\xi}$ *and observation times* $t' = t + \epsilon\tilde{t}$, *with* $t \leq t^\star$, *we get*

$$\lim_{\epsilon\to 0} E\left\{D(t,\mathbf{h})D\left(t+\epsilon\tilde{t},\mathbf{h}+\epsilon\boldsymbol{\xi}\right)\right\} = \frac{1}{4(2\pi)^3}\int_{-\infty}^{\infty} d\omega\,\omega^2 \int_0^{K_{t^\star}} dK\,\frac{K}{h}\,|\hat{\varphi}(\omega,K\mathbf{e}_0)|^2 \\ W_1(\omega,K,t,h,0)\cos\left[\omega(\tilde{t}-K\xi)\right]. \tag{3.3}$$

Here $h = |\mathbf{h}|$, $\xi = |\boldsymbol{\xi}|$, $\mathbf{e}_\theta = (\cos\theta,\sin\theta)$ *and the upper bound* $K_{t^\star} = 1/\max_{z>-\mathcal{L}_{t^\star}} c(z)$ *in the slowness integral ensures that we have propagating plane waves with real and positive vertical speed* $c(K,z)$. *The intensity of the backscattered field follows from (3.3), in the case* $\tilde{t} = 0$ *and* $\boldsymbol{\xi} = \mathbf{0}$,

$$\lim_{\epsilon\to 0} E\left\{[D(t,\mathbf{h})]^2\right\} = \frac{1}{4(2\pi)^3}\int_{-\infty}^{\infty} d\omega\,\omega^2 \int_0^{K_{t^\star}} dK\,\frac{K}{h}\,|\hat{\varphi}(\omega,K\mathbf{e}_0)|^2 W_1(\omega,K,t,h,0). \tag{3.4}$$

Proof: We begin with expression (2.30) of the data, which we rewrite in polar coordinates

$$D(t,\mathbf{h}) = \frac{1}{2(2\pi)^3\epsilon^{3/2}}\int_{-\infty}^{\infty} d\omega \int_0^{K_{t^\star}} dK\,\omega^2 K \int_0^{2\pi} d\theta\,\hat{\varphi}(\omega,K\mathbf{e}_\theta)\,\mathcal{R}_{t^\star}^\epsilon(\omega,K,0)e^{-i\frac{\omega}{\epsilon}t + i\frac{\omega}{\epsilon}Kh\cos\theta}, \tag{3.5}$$

with angle θ measured with respect to the direction of $\mathbf{h}$. Recall from Lemma 2.1 the rapid decorrelation of $\mathcal{R}_{t^\star}^\epsilon$ over ω and K, and assume a smooth pulse shape $\hat{\varphi}$, to get

$$E\left\{D(t,\mathbf{h})D\left(t',\mathbf{h}'\right)\right\} = \frac{1}{4(2\pi)^6\epsilon}\int_{-\infty}^{\infty} d\omega \int_o^{K_{t^\star}} dK\,\omega^4K^2 \int_{-\infty}^{\infty} d\tilde{\omega}\int_{-\infty}^{\infty} d\tilde{K}E\left\{\mathcal{R}_{t^\star}^\epsilon\left(\omega+\frac{\epsilon\tilde{\omega}}{2},K+\frac{\epsilon\tilde{K}}{2},0\right)\right. \\ \left.\overline{\mathcal{R}_{t^\star}^\epsilon\left(\omega-\frac{\epsilon\tilde{\omega}}{2},K-\frac{\epsilon\tilde{K}}{2},0\right)}\right\}\int_0^{2\pi} d\theta\,\hat{\varphi}(\omega,K\mathbf{e}_\theta)\int_0^{2\pi} d\theta'\,\overline{\hat{\varphi}(\omega,K\mathbf{e}_{\theta'})}\exp\left\{-i\frac{\omega}{\epsilon}(t-t')\right. \\ \left. + i\frac{\omega}{\epsilon}K(h\cos\theta - h'\cos\theta') + i(\omega\tilde{K}+\tilde{\omega}K)\frac{(h\cos\theta+h'\cos\theta')}{2} - i\tilde{\omega}\frac{(t+t')}{2}\right\} + \ldots,$$

where we denote by "..." the lower order terms.

We deal first with the $O(1/\epsilon)$ phase, and then take the limit (2.38). The fast phase depends on the variables $\omega, K, \theta, \theta'$ and the leading order contribution comes from the vicinity of the stationary points satisfying equations

$$\begin{aligned} t - t' - K(h\cos\theta - h'\cos\theta') &= 0, \\ \omega\,(h\cos\theta - h'\cos\theta') &= 0, \\ \omega K h \sin\theta = \omega K h' \sin\theta' &= 0. \end{aligned}$$

It is easy to see that there are no stationary points if $|t-t'|/t^\star > O(\epsilon)$. In the case $|t-t'|/t^\star \leq O(\epsilon)$, but $|h-h'|/a > O(\epsilon)$, the stationary point is at $\omega = 0$ and $K = 0$ and it makes no contribution to the cross correlation, because of the amplitude factor $\omega^4 K^2$. Thus, $E\left\{D(t,\mathbf{h})D\left(t',\mathbf{h}'\right)\right\}$ is small for $|\mathbf{h}-\mathbf{h}'|/a > O(\epsilon)$ and/or $|t-t'|/t^\star > O(\epsilon)$ and it tends to zero as $\epsilon \to 0$.

Let then $\mathbf{h}' = \mathbf{h} + \epsilon\boldsymbol{\xi}$, $t' = t + \epsilon\tilde{t}$, and observe that now we have stationary points for $\theta = \theta' = 0$ or π, with no restriction on ω and K. Integrating over θ and θ', we obtain

$$E\left\{D(t,\mathbf{h})D\left(t+\epsilon\tilde{t},\mathbf{h}+\epsilon\boldsymbol{\xi}\right)\right\} = \frac{1}{4(2\pi)^5}\int_{-\infty}^{\infty} d\omega \int_o^{K_{t^\star}} dK\,|\omega|^3 \frac{K}{h}\sum_{q=\pm 1}|\hat{\varphi}(\omega, qK\mathbf{e}_0)|^2 \int_{-\infty}^{\infty} d\tilde{\omega}\int_{-\infty}^{\infty} d\tilde{K}$$
$$E\left\{\mathcal{R}^\epsilon_{t^\star}\left(\omega+\frac{\epsilon\tilde{\omega}}{2}, K+\frac{\epsilon\tilde{K}}{2}, 0\right)\overline{\mathcal{R}^\epsilon_{t^\star}\left(\omega-\frac{\epsilon\tilde{\omega}}{2}, K-\frac{\epsilon\tilde{K}}{2}, 0\right)}\right\} e^{i\omega[\tilde{t}-qK\xi]+i(\omega\tilde{K}+\tilde{\omega}K)qh-i\tilde{\omega}t} + \dots.$$

Next, we use Lemma 2.1 for the limit $\epsilon \to 0$ of $E\left\{\mathcal{R}^\epsilon_{t^\star}\overline{\mathcal{R}^\epsilon_{t^\star}}\right\}$,

$$\lim_{\epsilon\to 0} E\left\{D(t,\mathbf{h})D\left(t+\epsilon\tilde{t},\mathbf{h}+\epsilon\boldsymbol{\xi}\right)\right\} = \frac{1}{4(2\pi)^5}\int_{-\infty}^{\infty} d\omega \int_o^{K_{t^\star}} dK\,|\omega|^3 \frac{K}{h}\sum_{q=\pm 1}|\hat{\varphi}(\omega, qK\mathbf{e}_0)|^2 e^{i\omega[\tilde{t}-qK\xi]}\int_{-\infty}^{\infty} d\tilde{\omega}$$
$$\int_{-\infty}^{\infty} d\tilde{K}\int_{-\infty}^{\infty} ds\int_{-\infty}^{\infty} d\chi\, W_1(\omega,K,s,\chi,0)\exp\left\{i\tilde{\omega}(s-K\chi) - i\omega\tilde{K}\chi + i(\omega\tilde{K}+\tilde{\omega}K)qh - i\tilde{\omega}t\right\}$$

and we integrate over $\tilde{\omega}$ and $\tilde{K}$ to get

$$\lim_{\epsilon\to 0} E\left\{D(t,\mathbf{h})D\left(t+\epsilon\tilde{t},\mathbf{h}+\epsilon\boldsymbol{\xi}\right)\right\} = \frac{1}{4(2\pi)^3}\int_{-\infty}^{\infty} d\omega\,|\omega|^3 \int_o^{K_{t^\star}} dK\,\frac{K}{h}\sum_{q=\pm 1}|\hat{\varphi}(\omega, qK\mathbf{e}_0)|^2 e^{i\omega(\tilde{t}-qK\xi)}$$
$$\int_{-\infty}^{\infty} ds\int_{-\infty}^{\infty} d\chi\, W_1(\omega,K,s,\chi,0)\delta[s-t+K(qh-\chi)]\,\delta[\omega(qh-\chi)].$$

It turns out (see section 3.3) that $W_1(\omega,K,s,\chi,0)$ is even in ω and that it is supported on $\chi > 0$, so only $q=1$ contributes in the sum. The result (3.3) follows from the properties of Dirac δ distributions. □

3.2. Layer annihilator filters. The intensity (3.4) of the incoherent field stays $O(1)$ as $t^\star$ (i.e., $\mathcal{L}_{t^\star}$) increases, whereas the intensity of the coherent echoes decreases exponentially with depth. This is why we have low SNR at the array when imaging objects buried deep in the random medium. The filters described in this section seek to improve the SNR by annihilating the layer echoes. Their design involves ideas that are common in exploration geophysics, such as normal move-out, gather flattening [14] and differential semblance velocity estimation [12, 25]. All these methods are based on the single scattering approximation, and so are the filters, intended to remove the *primary echoes* that went through a *single* reflection at some layer in the

medium. It is therefore unexpected that, as shown in sections 3.3 and 4, the filters annihilate the incoherent echoes produced by the random medium, where multiple reflections dominate.

As a preparatory step in defining the filters, imagine that we had a *single layer* at depth $z < 0$, embedded in a *smooth* medium with speed $c(z)$. Then, we would receive at offset $\mathbf{h}$ and time $T_c(h, z)$ the echo[‖]

$$D_o(t, \mathbf{h}; z) \approx \frac{\epsilon^{\frac{3}{2}}}{2(2\pi)^3} \int \frac{d\omega}{\epsilon} \int d\mathbf{K} \left(\frac{\omega}{\epsilon}\right)^2 \hat{\varphi}(\omega, \mathbf{K})\, R(\omega, K; z) e^{-i\frac{\omega}{\epsilon}[t+2\tau(K,z)]+i\frac{\omega}{\epsilon}\mathbf{K}\cdot\mathbf{h}}, \tag{3.6}$$

with amplitude modulated by $R(\omega, K; z)$, the reflection coefficient of the layer. The arrival time $T_c(h, z)$ is determined by the method of stationary phase applied to the ω and $\mathbf{K}$ integrals in (3.6):

$$T_c(h, z) = -2\tau(K_c, z) + hK_c = 2\int_{-|z|}^{0} \frac{dz'}{c(z')\sqrt{1 - c^2(z')K_c^2}}, \tag{3.7}$$

where

$$\frac{h}{2} = K_c \int_{-|z|}^{0} \frac{c(z')}{\sqrt{1 - c^2(z')K_c^2}} dz'. \tag{3.8}$$

Note that the right hand side in (3.8) is monotonically increasing with K_c, and that we have the identity

$$K_c = \frac{d}{dh} T_c(h, z). \tag{3.9}$$

Thus, there is a unique slowness K_c and a unique arrival time $T_c(h, z)$, for each z. For example, in the homogeneous case $c(z) = c_o$, equations (3.7)-(3.9) take the explicit form

$$K_{c_o} = \frac{h}{c_o\sqrt{h^2 + 4z^2}} = \frac{h}{c_o^2 T_{c_o}(h, z)} \quad \text{and} \quad T_{c_o}(h, z) = \frac{\sqrt{h^2 + 4z^2}}{c_o}. \tag{3.10}$$

The layer annihilator filters are designed to remove arrivals at times (3.7), for all $z < 0$. Since in applications we may not know the background speed $c(z)$, we define the filters at a trial speed $\tilde{c}(z)$. Then, we show with numerical simulations in section 4 that the filters can be used to estimate $c(z)$.

DEFINITION 3.2. *Let $T_{\tilde{c}}(h, z)$ be the travel time function (3.7) at the trial speed $\tilde{c}$. This function is monotonically increasing with $|z|$, so we can define the negative valued inverse function $\zeta_{\tilde{c}}(h, t)$, satisfying*

$$T_{\tilde{c}}\left(h, \zeta_{\tilde{c}}(h, t)\right) = t, \quad \zeta_{\tilde{c}}\left(h, T_{\tilde{c}}(h, z)\right) = z. \tag{3.11}$$

For example, in the homogeneous case $c = c_o$, we have $\zeta_{c_o}(h, t) = -\sqrt{c_o^2 t^2 - h^2}/2$. We define the filters $\mathbb{Q}_{\tilde{c}}$ as linear operators that take the data $D(t, \mathbf{h})$ and map it to

$$\mathbb{Q}_{\tilde{c}} D(t, \mathbf{h}) = \left\{ D\left(T_{\tilde{c}}(h, z), \mathbf{h}\right) - \frac{1}{a^\epsilon} \int_{h-\frac{a^\epsilon}{2}}^{h+\frac{a^\epsilon}{2}} D\left(T_{\tilde{c}}(h', z), \mathbf{h}'\right) dh' \right\}_{z=\zeta_{\tilde{c}}(h,t).} \tag{3.12}$$

Here $\mathbf{h}$ and $\mathbf{h}'$ are collinear offset vectors with magnitudes h and h' separated by at most a^ϵ, a local aperture that may depend on ϵ.

The choice of a^ϵ is discussed in the next section, where we show that the annihilators work when $a^\epsilon \sim \lambda_o^\epsilon$. This means that the filtering should be done locally, in neighborhoods of a few wavelengths around each receiver location.

[‖]Equation (3.6) is obtained easily with the techniques described in section 2 and it can be found in [21, 8].

Now let us explain Definition 3.2, which involves three essential steps: (1) The mapping of the data from the $(t, \mathbf{h})$ space to the depth and offset space $(z, \mathbf{h})$, using the travel time $T_{\tilde{c}}(h, z)$. This is called normal move-out in the geophysics literature [14, 4]. (2) The annihilation step is the subtraction of the local average of the data, after normal-moveout. If we had indeed echoes arriving at times $T_{\tilde{c}}(h, z)$, this subtraction would remove them. (3) In the last step we return to the $(t, \mathbf{h})$ space, using the inverse function $\zeta_{\tilde{c}}(h, t)$.

There are other ways to do the annihilation. For example, in [8] we studied the choice $\frac{d}{dh} D\left(T_{\tilde{c}}(h, z), \mathbf{h}\right)$, motivated by the differential-semblance velocity methods [12, 25]. The "differential semblance filters" deal well with the "noise" from the layers, but they require additional smoothing when the data is polluted by other sources of noise. We showed in [8] that subtracting the average of the traces after normal move-out, as in Definition 3.2, gives a robust annihilation that can handle noise, including clutter "noise" due to scattering by weak and small inhomogeneities embedded in the layered medium.

3.3. Intensity of the backscattered field after the annihilation. Our goal in this section is to compute the intensity $E\left\{\left[\mathbb{Q}_{\tilde{c}} D(t, \mathbf{h})\right]^2\right\}$ of the filtered data and to compare it with (3.4). We say that the annihilation is successful if $E\left\{\left[\mathbb{Q}_{\tilde{c}} D(t, \mathbf{h})\right]^2\right\} \ll E\left\{\left[D(t, \mathbf{h})\right]^2\right\}$, and this should depend on how close the trial $\tilde{c}(z)$ is to the true speed $c(z)$.

Let us take collinear offsets $\mathbf{h}$ and $\mathbf{h}'$ and define

$$\mathcal{D}_{\tilde{c}}(t, \mathbf{h}, \mathbf{h}') = \left\{D\left(T_{\tilde{c}}(h, z), \mathbf{h}\right) - D\left(T_{\tilde{c}}(h', z), \mathbf{h}'\right)\right\}_{z=\zeta_{\tilde{c}}(h,t)}. \tag{3.13}$$

Then, it is sufficient to estimate the intensity $E\left\{\left[\mathcal{D}_{\tilde{c}}(t, \mathbf{h}, \mathbf{h}')\right]^2\right\}$, because

$$E\left\{\left[\mathbb{Q}_{\tilde{c}} D(t, \mathbf{h})\right]^2\right\} = E\left\{\left[\frac{1}{a^\epsilon}\int_{h-\frac{a^\epsilon}{2}}^{h+\frac{a^\epsilon}{2}} \mathcal{D}_{\tilde{c}}(t, \mathbf{h}, \mathbf{h}') dh'\right]^2\right\} \leq \frac{1}{a^\epsilon}\int_{h-\frac{a^\epsilon}{2}}^{h+\frac{a^\epsilon}{2}} E\left\{\left[\mathcal{D}_{\tilde{c}}(t, \mathbf{h}, \mathbf{h}')\right]^2\right\} dh', \tag{3.14}$$

by the Cauchy-Schwartz inequality. We have the following result:

THEOREM 3.3. *The annihilation filters require local apertures $a^\epsilon \sim \lambda_o^\epsilon$ in Definition 3.2, because*

$$E\left\{\left[\mathcal{D}_{\tilde{c}}(t, \mathbf{h}, \mathbf{h}')\right]^2\right\} \approx E\left\{\left[D\left(T_{\tilde{c}}(h, z), \mathbf{h}\right)\right]^2\right\} + E\left\{\left[D\left(T_{\tilde{c}}(h', z), \mathbf{h}'\right)\right]^2\right\},$$

if $|\mathbf{h} - \mathbf{h}'| \gg \lambda_o^\epsilon$. When $\mathbf{h}' = \mathbf{h} + \epsilon\boldsymbol{\xi}$, and $\boldsymbol{\xi}$ is collinear with $\mathbf{h}$, we have

$$\lim_{\epsilon\to 0} E\left\{\left[\mathcal{D}_{\tilde{c}}(t, \mathbf{h}, \mathbf{h} + \epsilon\boldsymbol{\xi})\right]^2\right\} = \frac{1}{2(2\pi)^3}\int_{-\infty}^{\infty} d\omega\, \omega^2 \int_0^{K_{t^\star}} dK\, \frac{K}{h}\, |\hat{\varphi}(\omega, K\mathbf{e}_0)|^2 \\ W_1(\omega, K, t, h, 0)\left\{1 - \cos\left[\omega\xi(K_{\tilde{c}} - K)\right]\right\}, \tag{3.15}$$

so the success of the annihilation depends on the spread of the support of W_1 around the slowness K_c.

In the particular case of constant mean speed $c(z) = c_o$, we get perfect annihilation in the limit, because

$$\lim_{\epsilon\to 0} E\left\{\left[\mathcal{D}_{c_o}(t, \mathbf{h}, \mathbf{h} + \epsilon\boldsymbol{\xi})\right]^2\right\} = 0, \quad \textit{and therefore} \quad \lim_{\epsilon\to 0} E\left\{\left[\mathbb{Q}_{c_o} D(t, \mathbf{h})\right]^2\right\} = 0. \tag{3.16}$$

Moreover, we can estimate c_o by minimizing over $\tilde{c}$ the energy after the annihilation

$$\int_{t\leq t^\star} dt \int_{|\mathbf{h}|\leq a/2} d\mathbf{h}\, \left[\mathbb{Q}_{\tilde{c}} D(t, \mathbf{h})\right]^2$$

since

$$\lim_{\epsilon \to 0} E\left\{ [\mathbb{Q}_{\tilde{c}} D(t, \mathbf{h})]^2 \right\} = O(\gamma), \tag{3.17}$$

for trial speeds satisfying the uniform error bound $\frac{|\tilde{c}(z)-c_o|}{c_o} \leq \gamma$ *for all* $z \leq 0$.

Proof: The proof relies on the probabilistic representation of the solution $W_1(\omega, K, t, h, 0)$ of transport equations (2.39). This takes a simple form when $c(z) = c_o$, and we get the explicit result (3.16). We discuss briefly, after the proof of the theorem, extensions to small magnitude variations of $c(z)$. Then, we use numerical simulations in section 4, to illustrate the annihilation for general speeds.

That no annihilation occurs when $|\mathbf{h} - \mathbf{h}'| \gg \lambda_o^\epsilon$, can be seen easily from definition (3.13) and the rapid decorrelation of the incoherent field stated in Lemma 3.1. Take then $\mathbf{h}' = \mathbf{h} + \epsilon\boldsymbol{\xi}$, with collinear $\boldsymbol{\xi}$ and $\mathbf{h}$, and use equation (3.9) to write

$$T_{\tilde{c}}(h', z) \approx T_{\tilde{c}}(h, z) + \epsilon K_{\tilde{c}} \xi, \quad \xi = |\boldsymbol{\xi}|, \tag{3.18}$$

for $z = \zeta_{\tilde{c}}(h, t)$. We obtain from Lemma 3.1 and the smoothness [**] of the intensity function (3.4) that

$$\lim_{\epsilon \to 0} E\left\{ [D\left(T_{\tilde{c}}(h, z), \mathbf{h}\right) - D\left(T_{\tilde{c}}(h, z) + \epsilon K_{\tilde{c}} \xi, \mathbf{h} + \epsilon\boldsymbol{\xi}\right)]^2 \right\} = \frac{1}{2(2\pi)^3} \int_{-\infty}^{\infty} d\omega\, \omega^2 \int_0^{K_{t^\star}} dK\, \frac{K}{h}\, |\hat{\varphi}(\omega, K\mathbf{e}_0)|^2$$
$$W_1(\omega, K, T_{\tilde{c}}(h, z), h, 0)\left\{1 - \cos\left[\omega\xi(K_{\tilde{c}} - K)\right]\right\}. \tag{3.19}$$

Equation (3.15) follows by setting $z = \zeta_{\tilde{c}}(h, t)$, since $T_{\tilde{c}}(h, \zeta_{\tilde{c}}(h, t)) = t$, by definition.

To complete the proof we look at the dependence of $W_1(\omega, K, t, h, 0)$ on the slowness K, using the probabilistic representation of the solution of transport equations (2.39). Let us define $\{n(\mathcal{Z})\}_{\mathcal{Z} \geq \mathcal{Z}_{t^\star}}$, a Markov jump process with state space on the positive integers, and with dimensionless depth argument

$$\mathcal{Z}(z) = \int_0^z \frac{dz'}{L_{loc}(\omega, K, z')}, \tag{3.20}$$

scaled by the localization length $L_{loc}(\omega, K, s)$. Here $z > -\mathcal{L}_{t^\star}$ and $\mathcal{Z}_{t^\star} = \mathcal{Z}(-\mathcal{L}_{t^\star})$. The process $n(\mathcal{Z})$ has an absorbing state at $N = 0$ and it jumps from states $N > 0$ to $N \pm 1$, with equal probability $1/2$. The jumps occur at random depths, with exponential distribution and parameter $2N^2$.

The probabilistic representation of W_1 in terms of $n(\mathcal{Z})$ is in the next lemma. The result follows from Feynman-Kac's formula [11] and it is derived in [1, 21]. We review the derivation briefly in Appendix A.

LEMMA 3.4. *The solution* $W_1(\omega, K, s, \chi, 0)$ *of transport equations (2.39), evaluated at* $z = 0$*, is given by*

$$W_1(\omega, K, s, \chi, 0) = E_1\left\{ \delta_{0,n(0)}\, \delta\left[s - \int_{-\mathcal{L}_{t^\star}}^0 \frac{2n(\mathcal{Z}(z'))}{c(z')\sqrt{1 - c^2(z')K^2}} dz' \right] \delta\left[\chi - \int_{-\mathcal{L}_{t^\star}}^0 \frac{2n(\mathcal{Z}(z'))Kc(z')}{\sqrt{1 - c^2(z')K^2}} dz' \right] \right\}, \tag{3.21}$$

where E_1 *denotes the expectation conditioned by* $n(\mathcal{Z}_{t^\star}) = 1$.

Note that $W_1(\omega, K, s, \chi, 0)$ depends on ω^2 through the localization length L_{loc}, and it is supported on the positive χ and s, as stated in the proof of Lemma 3.1. Note also that $n(\mathcal{Z})$ must be in the absorbing

[**]The smoothness of $E\left\{[D(t, \mathbf{h})]^2\right\}$ with respect to t and $\mathbf{h}$, can be inferred from [21, 1] and from the calculation below.

state 0 when $\mathcal{Z}=0$ (i.e., $z=0$), in order to participate in (3.21). The artificial depth $\mathcal{L}_{t^\star}$ is introduced for technical reasons and we conclude from its definition that

$$t^\star \le 2\int_{-\mathcal{L}_{t^\star}}^{0} \frac{dz'}{c(z')\sqrt{1-c^2(z')K^2}}, \quad \text{for all } K\in[0,K_{t^\star}].$$

In Theorem 3.3 we need $W_1(\omega,K,s,\chi,0)$ at $s=t<t^\star$, so the first Dirac δ in (3.21) acts on the trajectories $n(\mathcal{Z}(z))$ that are absorbed by state 0 at some depth $z<0$. Thus, we may drop $\delta_{0,n(0)}$ in (3.21), and note that W_1 is independent of $t^\star$, as long as we observe it at times $s=t<t^\star$. In particular, we may let $t^\star\to\infty$ and work with the process $n(\mathcal{Z})$ in the half space $\mathcal{Z}\le 0$.

When the background is homogeneous, (3.21) simplifies to

$$W_1(\omega,K,s,\chi,0) = E_1\left\{\delta\left[s-\frac{2\overline{n}}{c_o\sqrt{1-c_o^2K^2}}\right]\delta\left[\chi-\frac{2\overline{n}Kc_o}{\sqrt{1-c_o^2K^2}}\right]\right\},$$

and it depends on a single random variable

$$\overline{n}=\int_{-\infty}^{0} n(\mathcal{Z}(z'))dz',$$

that can be eliminated from the second Dirac δ to obtain

$$W_1(\omega,K,s,\chi,0) = E_1\left\{\delta\left[s-\frac{2\overline{n}}{c_o\sqrt{1-c_o^2K^2}}\right]\right\}\delta\left[\chi-Kc_o^2 s\right].$$

Thus, $W_1(\omega,K,t,h,0)$ is supported on the slowness $K=h/(c_o^2t)=K_{c_o}$, and (3.15) becomes

$$\lim_{\epsilon\to 0} E\left\{\left[\mathcal{D}_{\tilde{c}}(t,\mathbf{h},\mathbf{h}+\epsilon\boldsymbol{\xi})\right]^2\right\} = \int_{-\infty}^{\infty} d\omega\,\frac{|\hat{\varphi}(\omega,K_{c_o}\mathbf{e}_0)|^2}{2(2\pi)^3c_o^4t^2}\mathcal{W}_1(\omega,K_{c_o},t)\left\{1-\cos\left[\omega\xi(K_{\tilde{c}}-K_{c_o})\right]\right\},$$

with $\mathcal{W}_1$ given by (see [1, 21] and Appendix A)

$$\mathcal{W}_1(\omega,K_{c_o},t) = E_1\left\{\delta\left[t-\frac{2\overline{n}}{c_o\sqrt{1-c_o^2K_{c_o}^2}}\right]\right\} = \frac{\omega^2 l}{2c_o\sqrt{1-c_o^2K_{c_o}^2}}\left[2+\frac{\omega^2 lt}{4c_o\sqrt{1-c_o^2K_{c_o}^2}}\right]^{-2}.$$

This is assuming that $h<c_ot$, so that K_{c_o} is in the domain of integration (i.e., $K_{c_o}<K_{t^\star}=1/c_o$). If this where not the case, then the intensity before and after annihilation would be zero in the limit.

Now let $\tilde{c}=c_o+O(\gamma c_o)$ and recall from (3.9) that $K_{\tilde{c}}$ changes smoothly with $\tilde{c}$. We conclude from the mean value theorem that

$$\lim_{\epsilon\to 0} E\left\{\left[\mathcal{D}_{\tilde{c}}(t,\mathbf{h},\mathbf{h}+\epsilon\boldsymbol{\xi})\right]^2\right\} = O(\gamma),$$

as stated in (3.17). □

Let us discuss briefly the case of small amplitude variations of $c(z)$,

$$c(z)=c_o+\gamma w(z), \tag{3.22}$$

where $\gamma\ll 1$ and $w(z)$ is a smooth function, bounded independently of γ. We get from Lemma 3.4, after expanding the integrands in series of γ, that

$$W_1(\omega,K,t,h,0) = E_1\left\{\delta\left[t-\int_{-\infty}^{0}\frac{2n(\mathcal{Z}(z'))}{c(z')\sqrt{1-c^2(z')K^2}}dz'\right]\delta\left[h-Kc_o^2t-\frac{4\gamma K}{\sqrt{1-c_o^2K^2}}\times\right.\right.$$
$$\left.\left.\int_{-\infty}^{0} n(\mathcal{Z}(z'))w(z')dz'+O(\gamma^2)\right]\right\}. \tag{3.23}$$

Here we let $\mathcal{L}_{t^\star} \to \infty$ and we used the first Dirac δ to rewrite the leading order term $h - Kc_o^2 t$ in the argument of the second one.

Now, w is bounded independently of γ, and since $n(\mathcal{Z}) \geq 0$, we have

$$\left| \int_{-\infty}^{0} n(\mathcal{Z}(z'))w(z')dz' \right| \leq \int_{-\infty}^{0} n(\mathcal{Z}(z'))|w(z')|dz' \leq C \int_{-\infty}^{0} \frac{n(\mathcal{Z}(z'))}{c(z')\sqrt{1-c^2(z')K^2}} dz' = \frac{Ct}{2}, \tag{3.24}$$

with constant C satisfying

$$|w(z)|c(z)\sqrt{1-c^2(z)K^2} \leq C, \quad \text{for all } z \leq 0.$$

The estimate (3.24) and equation (3.23) show that the support of $W_1(\omega, K, t, h, 0)$ in K is confined to an $O(\gamma)$ neighborhood of

$$K_{c_o} = \frac{h}{c_o^2 t} = K_{c_o + \gamma w} + O(\gamma),$$

and we can bound the intensity of the filtered echoes using (3.14) and (3.15),

$$E\left\{ [\mathbb{Q}_{c_o+\gamma w} D(t, \mathbf{h})]^2 \right\} \leq O(\gamma^2), \quad \text{as } \epsilon \to 0. \tag{3.25}$$

This bound is conservative, but it shows that the annihilation extends to variable speeds in a smooth manner. We illustrate next, with numerical simulations, the annihilation of the incoherent echoes produced by randomly layered media with general, variable mean speed $c(z)$.

3.4. The coherent echoes after the annihilation. To see why the filters $\mathbb{Q}_c$ are useful in imaging, let us comment briefly on their effect on the coherent echoes arriving from the compact objects that we wish to image. For simplicity, we limit this discussion to the case $c(z) = c_o$.

As explained in section 2, the coherent echoes from points $\vec{\mathbf{y}} \in \mathcal{S}$ arrive at times $\tau_c(\vec{\mathbf{x}}_s, \vec{\mathbf{y}}, \vec{\mathbf{x}}_r)\,[1 + O(\epsilon)]$, where $\vec{\mathbf{y}} = (\mathbf{y}, \eta - L)$ and

$$\tau_{c_o}(\vec{\mathbf{x}}_s, \vec{\mathbf{y}}, \vec{\mathbf{x}}_r) \equiv \tau_{c_o}^{ODA}(\mathbf{h}, \vec{\mathbf{y}}) = \frac{1}{c_o}\left[\sqrt{(L-\eta)^2 + |\mathbf{x}_s - \mathbf{y}|^2} + \sqrt{(L-\eta)^2 + |\mathbf{x}_s + \mathbf{h} - \mathbf{y}|^2} \right].$$

Let φ^{ODA} be the pulse shape of these arrivals and recall from section 2.5.1 that the pulse width is $O(\epsilon)$. Let also the amplitude of these coherent echoes be comparable to that of the incoherent field, which is $O(1)$ in our scaling. This is the interesting low SNR regime where the annihilator filters are expected to be useful.

Theorem 3.3 shows that if we subtract two traces, at offsets h and $h' = h + \epsilon\xi$, after the normal moveout, we basically remove the incoherent field for $t \leq \tau_c^{\mathcal{S}}$. However, the coherent echoes are not removed by the subtraction,

$$\left\{ \varphi^{ODA}\left[\frac{T_{c_o}(h+\epsilon\xi, z) - \tau_{c_o}^{ODA}(\mathbf{h}+\epsilon\xi, \vec{\mathbf{y}})(1+O(\epsilon))}{\epsilon} \right] - \varphi^{ODA}\left[\frac{T_{c_o}(h, z) - \tau_{c_o}^{ODA}(\mathbf{h}, \vec{\mathbf{y}})(1+O(\epsilon))}{\epsilon} \right] \right\}_{z=\zeta_{c_o}(h,t)}$$
$$\approx \xi \left[K_{c_o} - \frac{d}{dh}\tau_{c_o}^{ODA}(\mathbf{h}, \vec{\mathbf{y}}) \right] (\varphi^{ODA})' \left[\frac{t - \tau_{c_o}^{ODA}(\mathbf{h}, \vec{\mathbf{y}})(1+O(\epsilon))}{\epsilon} \right] = O(1),$$

because $\tau_{c_o}^{ODA}(\mathbf{h}, \vec{\mathbf{y}})$ and $T_c(h, z)$ have different dependence on the offset. That is to say, for observation times $t = \tau_{c_o}^{ODA}(\mathbf{h}, \vec{\mathbf{y}})(1 + O(\epsilon))$ that are in the support of the coherent arrivals, we have

$$\frac{d}{dh}\tau_{c_o}^{ODA}(\mathbf{h}, \vec{\mathbf{y}}) = \frac{d\mathbf{h}}{dh} \cdot \frac{(\mathbf{x}_s + \mathbf{h} - \mathbf{y})}{\sqrt{(L-\eta)^2 + |\mathbf{x}_s + \mathbf{h} - \mathbf{y}|^2}} \neq K_{c_o} = \frac{h}{c_o^2 t}$$

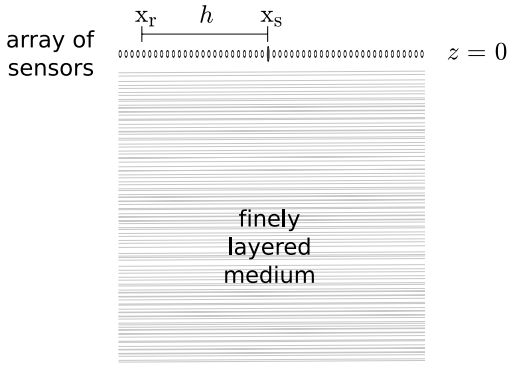

FIG. 4.1. *Illustration of the setup for the numerical simulations.*

in all cases except the special ones $\mathbf{y} = \mathbf{x}_s + \frac{\mathbf{h}}{2}(1 + O(\epsilon))$.

Thus, the filters are useful in imaging because they annihilate the "noise" (the incoherent field) but not the "signal" (the echoes from the objects that we wish to image).

4. Numerical results. We present numerical simulations in two dimensions, in the setup illustrated in Figure 4.1. The array consists of 81 receivers distributed uniformly, at distance $\lambda_o^\epsilon/2$ apart, in an interval of length $a = 40\lambda_o^\epsilon$. The source is at the center of the array and it emits downward a pulse $f(t)$, given by the derivative of a Gaussian. The central frequency is 30Hz and the bandwidth at 6dB is $20 - 40$Hz. The speed $v(z)$ varies around the scale $c_o = 3$km/s (see Figure 4.2).

We generate the rapid fluctuations of $v(z)$ using random Fourier series, with Gaussian correlation function $\mathcal{C}(z)$ and with correlation length of 2m. The strength of the fluctuations ranges from 13.3% to 50%. The central wavelength estimated at speed $c_o = 3$km/s is 100m and the distance of propagation is $L = 6$km. The setup is in agreement with the scaling in section 2.2, because

$$\epsilon \sim \frac{\ell^\epsilon}{\lambda_o^\epsilon} = 0.02 \sim \frac{\lambda_o^\epsilon}{L} = 0.017 \ll 1, \tag{4.1}$$

and σ is much larger than ϵ (i.e., it is $O(1)$).

We compute the data traces $P(t, \vec{\mathbf{x}}_r)$ by solving equations (2.1) with the mixed finite element time domain code ACOUST2D. This code implements the numerical method described in [2] and the finite elements are analyzed in [3]. The infinite extent of the medium is modeled numerically with a perfectly matched absorbing layer surrounding the computational domain [16].

The travel times $T_c(h, z)$ used in the normal move-out step in the annihilation process are obtained by solving equations (3.7)-(3.8). We use the MATLAB function *fzero* to find the slowness K_c from equation (3.8) and we evaluate the integrals in (3.7)-(3.8) with the MATLAB function *quadl*.

4.1. Imaging with layer annihilator filters. To illustrate the negative effects of backscattering when imaging in layered media, we present the results of a simulation with three small, acoustic soft scatterers buried at depth $L \sim 60\lambda_o^\epsilon$ in a finely layered medium. The scatterers are disks of radius λ_o^ϵ, and their centers are separated by $2.5\lambda_o^\epsilon$. The sound speed $v(z)$ is plotted in Figure 4.2, on the left.

We show in Figure 4.3 the time traces before and after the annihilation. The annihilator filter (3.12) is computed with the true mean speed and the local averaging aperture is $a^\epsilon = \lambda_o^\epsilon$. The recorded traces are

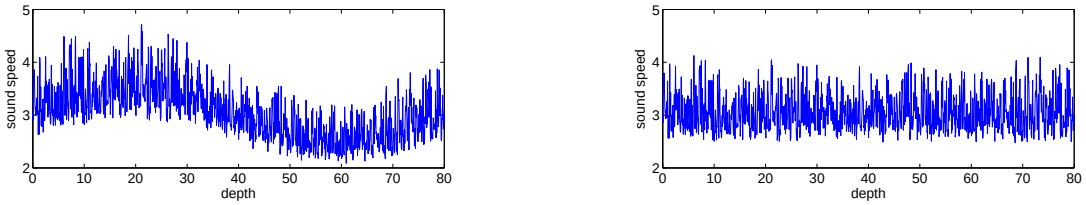

FIG. 4.2. *Sound speeds $v(z)$ considered in the numerical simulations of sections 4.1 and 4.2. We take three different strengths of the fine scale fluctuations:* 13%, 30% *and* 50%. *The plots are for* 30% *fluctuations. The depth z is in units of λ_o^ϵ and the speed is in units of km/s.*

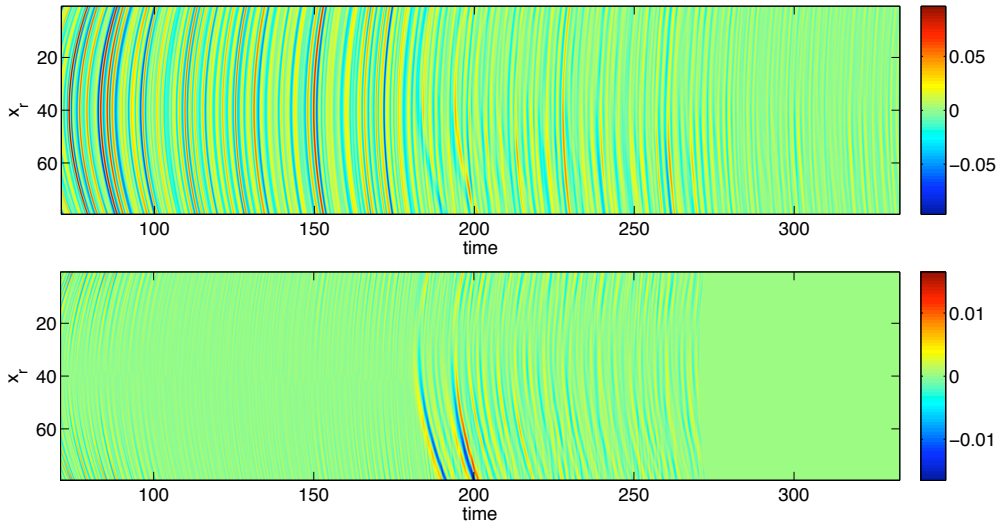

FIG. 4.3. *Top: Data traces in the medium with speed $v(z)$ plotted on the left in Figure 4.2. Bottom: The annihilated traces. The abscissa is time scaled by the pulse width and the ordinate is the receiver location scaled by λ_o^ϵ.*

dominated by the echoes from the layered medium, and the Kirchhoff migration image, shown on the left in Figure 4.4, is noisy and difficult to interpret. The imaging function is [4, 6, 13]

$$\mathcal{J}^{\mathrm{KM}}(\vec{\mathbf{y}}^s) = \sum_{\vec{\mathbf{x}}_r \in \mathcal{A}} P\big(\tau_c(\vec{\mathbf{x}}_r, \vec{\mathbf{y}}^s, \vec{\mathbf{x}}_s), \vec{\mathbf{x}}_r\big)$$

where $\vec{\mathbf{y}}^s$ is the search (image) point.

The filtered traces have a significantly higher SNR, as seen in the bottom plot of Figure 4.3. The amplitude of the backscattered echoes is much smaller after the annihilation and the coherent arrivals from the scatterers that we wish to image are emphasized. The image computed with the filtered data is shown in the right plot of Figure 4.4, and it is a clear improvement over the image shown on the left.

4.2. Annihilation in constant and variable backgrounds. Now we focus our attention on the subtraction $\mathcal{D}_c(t, h, h')$ of two traces, in media with constant and variable mean speeds $c(z)$. The realizations of $v(z)$ used in the simulations are shown in Figure 4.2, in the case of 30% strength of the fine scale fluctuations. We also consider weaker and stronger fluctuations of 13% and 50%, respectively.

First, we study the effect of the offset difference $h' - h$ on the amplitude of $\mathcal{D}_c(t, h, h')$, in the case of 30% fluctuations. Theorem 3.3 states that we should not get any annihilation if $|h' - h| > O(\lambda_o^\epsilon)$, and this

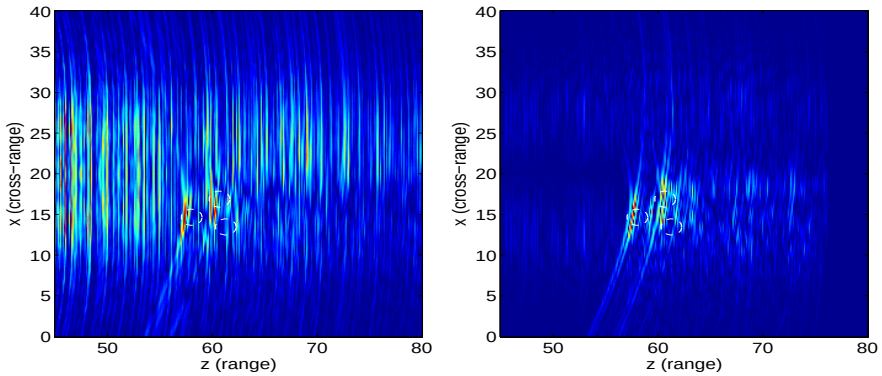

FIG. 4.4. *Left: Kirchhoff migration image obtained with the traces shown on the left in Figure 4.3. Right: image with the annihilated traces shown on the right in Figure 4.3. The range and cross-range is in units of λ_o^ϵ. The sound speed $v(z)$ is shown in the left plot of Figure 4.2. The location of the small scatterers is indicated with white circles.*

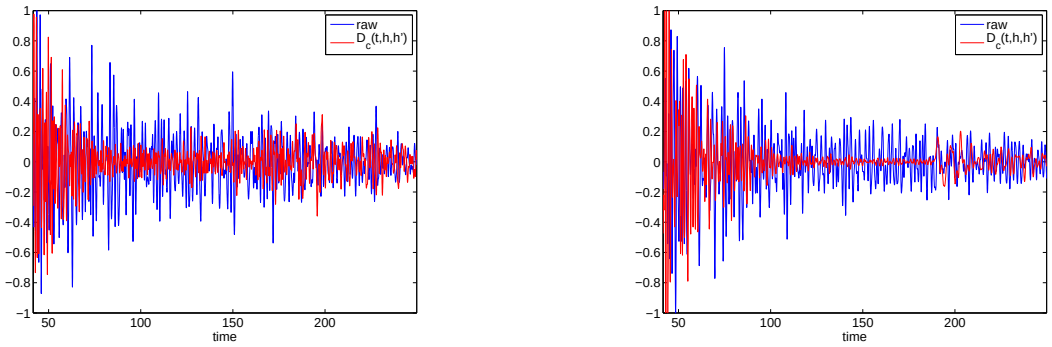

FIG. 4.5. *A recorded trace $D(t,h)$ (blue) and the subtracted traces $\mathcal{D}_c(t,h,h')$ (red), for offsets $h' = 15\lambda_o^\epsilon$ and $h = 0$. The mean speed is variable on the left column and constant on the right. The speeds $v(z)$ are plotted in Figure 4.2.*

is what we observe in Figure 4.5, where $h = 0$ and $h' = 15\lambda_o^\epsilon$. We plot in blue the trace $D(t, h = 0)$, and in red the subtraction of the traces $\mathcal{D}_c(t, h = 0, h' = 15\lambda_o^\epsilon)$. The trace $D(t, 0)$ is normalized by its maximum amplitude and we use the same normalization constant for the difference of the traces. We note from Figure 4.5 that there is no annihilation at the early times ($t \sim 50$ pulse widths, i.e., $\mathcal{L}_t \sim 15\lambda_o^\epsilon$), as expected, although some annihilation occurs at latter times, in the constant background case. In particular, we can see in the right plot of Figure 4.5 the coherent echoes from the small scatterers around time $t \sim 200$ pulse widths (i.e., $\mathcal{L}_t \sim 60\lambda_o$).

Next, we fix the offset difference $h' - h = 2.5\lambda_o^\epsilon$ and we plot with red lines in Figure 4.6, $D_c(t, h, h')$ for three values of h: 0, $5\lambda_o^\epsilon$ and $10\lambda_o^\epsilon$, respectively. The fluctuations of $v(z)$ are kept at 30%, as before. We note that the subtraction annihilates the incoherent echoes in both the variable and constant mean speed cases. The coherent arrivals around time $t = 200$ pulse widths are seen in all the red plots in Figure 4.6, but they could not be distinguished in the noisy traces shown in blue. The coherent arrivals are weaker in the small offset case, because the scatterers are placed almost beneath the source, and their cross-range is near the unfavorable position $\mathbf{x}_s + h/2$ described in section 3.4. The coherent arrivals are better seen at the larger offsets $h = 10\lambda_o$, but there we have less annihilation at the early times $t = 50$ pulse widths (i.e., $\mathcal{L}_t \sim 15\lambda_o^\epsilon \sim h = 10\lambda_o^\epsilon$).

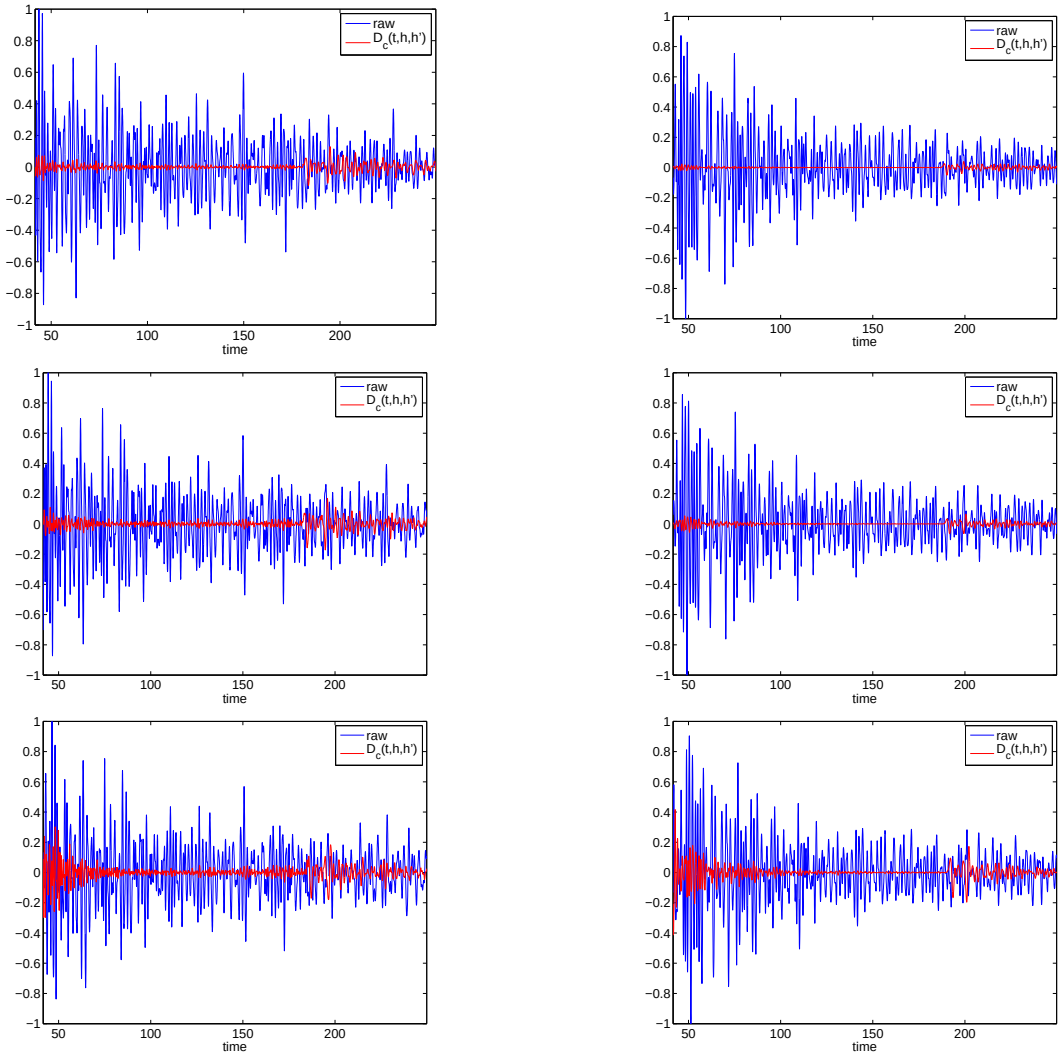

FIG. 4.6. *The recorded $D(t,h)$ (blue) and the subtracted traces $\mathcal{D}_c(t,h,h')$ (red). We have $h' = h + 2.5\lambda_o^\epsilon$, with $h = 0$ in the top row, $h = 5\lambda_o^\epsilon$ in the middle row and $h = 10\lambda_o^\epsilon$ in the bottom row. The mean speed is variable on the left column and constant on the right. The speeds $v(z)$ are plotted in Figure 4.2 and the fine scale fluctuations are 30%.*

Finally, we test the dependence of $D_c(t,h,h')$ on the strength of the fluctuations. We plot in Figure 4.7, with the red line, $D_c(t, h = 5\lambda_o^\epsilon, h' = 7.5\lambda_0^\epsilon)$ for 13%, and 50% fluctuations. The case of 30% fluctuations is in Figure 4.6. The plots are similar for the constant and variable mean speed $c(z)$, so we show only the variable case. We note that the annihilation of the incoherent echoes is almost independent of the strength of the fluctuations. However, the coherent echoes are weaker in the strongly fluctuating media, as expected. The stronger the fluctuations, the shorter the localization length, which means that we cannot image objects that are buried too deep in finely layered media.

4.3. Velocity estimation based on the annihilation filters. To estimate the mean speed, we minimize the energy of the annihilated traces over the trial speeds $\tilde{c}(z)$. Since the travel times change with $\tilde{c}$,

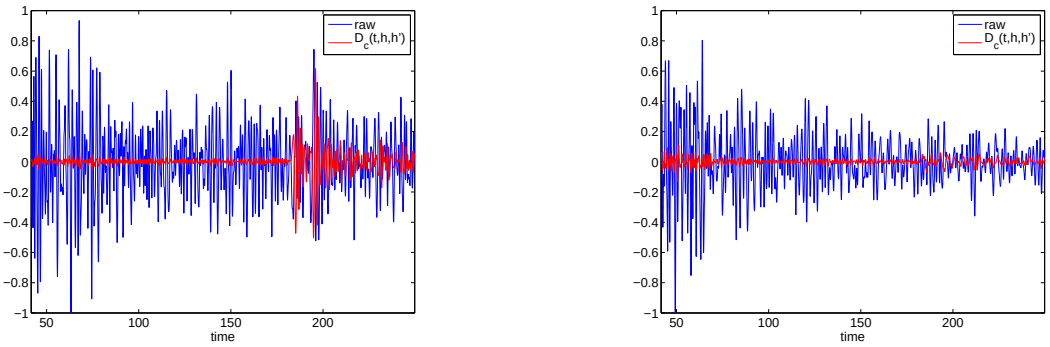

FIG. 4.7. *The recorded $D(t, h = 5\lambda_o^\epsilon)$ (blue) and the subtracted traces $\mathcal{D}_c(t, h = 5\lambda_o^\epsilon, h' = 7.5\lambda_o^\epsilon)$ (red). We have 13% fluctuations of $v(z)$ on the left and 50% on the right. The 30% case is shown in Figure 4.6. The mean speed is variable. The realization of $v(z)$ with 30% fluctuations is shown on the left in Figure 4.2.*

it is more convenient to work with the depth coordinate z instead of time, and define the objective function

$$\mathcal{O}(\tilde{c}) = \int_{-\mathcal{L}}^{0} dz \int_{|h|\leq \min\{|z|, a/2\}} dh \left| D(T_{\tilde{c}}(h,z),h) - \frac{1}{a^\epsilon} \int_{h-a^\epsilon/2}^{h+a^\epsilon/2} dh' D(T_{\tilde{c}}(h',z),h') \right|^2 , \tag{4.2}$$

for a maximum depth $-\mathcal{L}$. The local aperture is $a^\epsilon = \lambda_o^\epsilon$ and since we have data at finitely many offsets, we replace the integrals (4.2) with Riemann sums. The depth sampling is in steps of $\lambda_o^\epsilon/10$. We restrict in (4.2) the offsets by $|z|$, because geometrical spreading effects are strong when $h > |z|$ and the annihilation is not efficient, as it is based only on arrival times.

The unknown $\tilde{c}(z)$ is parametrized by its values at depths $z = -10j\lambda_o^\epsilon$, with $j = 0, 1, \ldots$. The field $\tilde{c}(z)$ is the cubic spline interpolation of these values. We optimize first over the depth interval $z \in (-40\lambda_o^\epsilon, 0)$. Then, we fix the speed up to $z = -30\lambda_o^\epsilon$, and we seek in the second step $\tilde{c}(z)$ for $z \in (-60\lambda_o^\epsilon, -30\lambda_o^\epsilon)$. We find that the speeds in the second interval affect very little the objective function. This is to be expected, because the depths in this interval are larger than the array aperture and the traces look flat after the normal move-out, for a wide range of trial speeds. We need a larger aperture to gain sensitivity of the objective function to $\tilde{c}$ at large depths.

We minimized (4.2) with the MATLAB function *fmincon*, and we constrained the trial speeds to the interval $[0.5c_m, 1.5c_M]$, where c_m and c_M are the minimum and maximum values of $c(z)$, respectively. Because of the weak sensitivity of the objective function to the speeds at depths $z \in (-60\lambda_o^\epsilon, -30\lambda_o^\epsilon)$, we regularized the second optimization by penalizing the square of the L_2 norm of the gradient of $\tilde{c}$. The regularization parameter was adjusted to balance the gradient of $\mathcal{O}(\tilde{c})$ with the gradient of the regularization term.

The results shown in Figure 4.8 fit well the actual mean speed, up to depth $z = -40\lambda_o^\epsilon$. We also show in Figure 4.9 the estimated mean speeds in media with stronger variations of $c(z)$, for depths above $-40\lambda_o^\epsilon$. Here we took a finer parametrization of $\tilde{c}(z)$, at depths $z = -2.67j\lambda_o^\epsilon$, with $j = 0, 1, \ldots 15$.

5. Summary and conclusions. Sensor array imaging in strongly backscattering media is complicated by a serious SNR issue: The coherent echoes from the scatterers that we wish to image are weak and they are difficult to extract from the noisy time traces recorded at the array. The question is how to filter out the backscattered echoes (the "noise") and thus improve the SNR, without knowing the medium in detail.

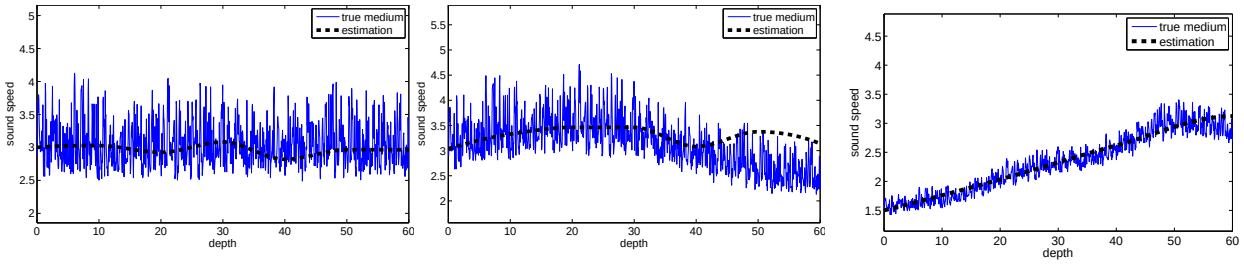

FIG. 4.8. *Velocity estimation results. We show with the blue solid line the true speed $v(z)$ and with the black dotted line the estimated $c(z)$. The abscissa is negative depth scaled by λ_o^ϵ and the speed is in units of km/s.*

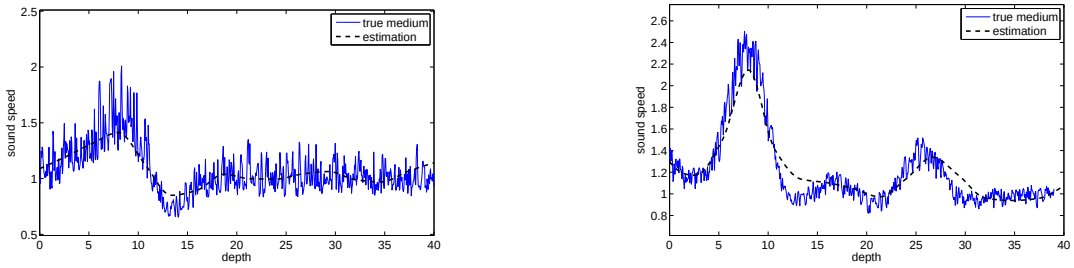

FIG. 4.9. *Velocity estimation in the case of stronger variation of the mean speed $c(z)$. We show with the blue solid line the true speed $v(z)$ and with the black dotted line the estimated $c(z)$. The abscissa is negative depth scaled by λ_o^ϵ and the speed is in units of km/s.*

This paper presents a theoretical and numerical study of such filters, for imaging in strongly backscattering, finely layered media. The study is based on the assumption of separation of scales. We consider a high frequency regime, with wavelengths that are small in comparisson with the large scales of variation in the medium. By fine layering, we mean that the wave speed fluctuates at small, sub wavelength scales. These rapid fluctuations are strong, and because they are unknown and they cannot be estimated from the array data, we model them with random processes.

Randomly layered media are an interesting case study, because they give a worse case scenario in terms of difficulties raised by clutter "noise". In particular, they cause wave localization, which means that as the waves propagate through the medium, they loose coherence exponentially fast, and imaging cannot be done beyond certain depths, called localization lengths. The backscattering adds up over such depths and all the energy is transfered to the incoherent part of the field, observed at the array in the form of long and noisy time traces (coda).

The layer annihilator filters considered in this paper are easy to implement, they are computationally cheap, and they do not require much data. The annihilation process involves commonly used techniques in exploration geophysics, such as normal move-out and semblance velocity estimation. These techniques are based on the single scattering approximation in the medium, and so are the filters. It is therefore remarkable that they can suppress the incoherent echoes produced by random media, as we have shown with analysis and numerical simulations.

The large scale features of the wave speed determine the travel times, and they enter explicitly in the definition of the filters. If they are not known, we must do a velocity estimation. It follows from the analysis

in the paper that the velocity estimation can be done in conjunction with the filtering process, at least in the case of constant or nearly constant mean speeds. The result seems to extend to more general, variable backgrounds, as we have shown with numerical simulations.

Acknowledgments. The work of L. Borcea and F. González del Cueto was partially supported by the Office of Naval Research, under grant N00014-05-1-0699 and by the National Science Foundation, grants DMS-0604008, DMS-0305056, DMS-0354658. The work of G. Papanicolaou was partially supported by US Army grant W911NF-07-2-0027-1, ONR grant N00014-02-1-0088, and AFOSR grant FA9550-08-1-0089. The work of C. Tsogka was partially supported by the European FP7 Marie Curie International Reintegration Grant MIRG-CT-2007-203438.

Appendix A. Probabilistic representation of the transport equations. We review briefly, from [1, 21], the probabilistic representation of the solution of the transport equations (2.39).

Let us begin with the change of variables (3.20), and remark that $\mathcal{Z}(z)$ is a monotonically increasing function of z. Thus, we may define the inverse map $z = g(\mathcal{Z})$, satisfying

$$g(\mathcal{Z}(z)) = z, \quad \frac{dg(\mathcal{Z})}{d\mathcal{Z}} = L_{loc}(\omega, K, g(\mathcal{Z})), \tag{A.1}$$

and we let

$$c_g(\mathcal{Z}) = [c \circ g](\mathcal{Z}) = c\left(g(\mathcal{Z})\right). \tag{A.2}$$

The transport equations (2.39) become

$$\frac{\partial W_N}{\partial \mathcal{Z}} + 2N\left[\frac{L_{loc}}{c_g\sqrt{1-c_g^2K^2}}\frac{\partial W_N}{\partial s} + \frac{L_{loc}c_gK}{\sqrt{1-c_g^2K^2}}\frac{\partial W_N}{\partial \chi}\right] = N^2\left(W_{N+1} - 2W_N + W_{N-1}\right), \quad \mathcal{Z} > \mathcal{Z}_{t^\star},$$
$$W_N = \delta_{0,N}\delta(s)\delta(\chi), \quad \mathcal{Z} = \mathcal{Z}_{t^\star}, \tag{A.3}$$

and we wish to solve them using the Markov jump process $\{n(\mathcal{Z})\}_{\mathcal{Z}\geq\mathcal{Z}_{t^\star}}$ defined in section 3.3.

To compute the infinitesimal generator $\mathbb{G}$ of the jump process,

$$\mathbb{G}\psi(N) = \lim_{\eta\to 0}\frac{1}{\eta}\left[E\left\{\psi\left(n(\mathcal{Z}+\eta)\right)|n(\mathcal{Z}) = N\right\} - \psi(N)\right],$$

we recall the following basic facts: (1) The jump times must be exponentially distributed for the process to be Markovian [18, section XVII.6]. In our case we let $2N^2$ be the parameter in the exponential distribution of the jump times, from state $N > 0$. (2) The probability that we have one jump in the interval $[\mathcal{Z}, \mathcal{Z}+\eta]$ is $2N^2\eta + o(\eta)$, as shown in [18, section XVII.2]. The jump is to $N \pm 1$ with equal probability $1/2$, by definition of the process. (3) The probability of more jumps is $o(\eta)$ and the probability of no jump is $e^{-2N^2\eta} = 1 - 2N^2\eta + o(\eta)$. Using these facts in the definition of $\mathbb{G}$, we obtain

$$\begin{aligned}\mathbb{G}\psi(N) &= \lim_{\eta\to 0}\frac{1}{\eta}\left[\psi(N+1)N^2\eta + \psi(N-1)N^2\eta + \psi(N)\left(1-2N^2\eta\right) + o(\eta) - \psi(N)\right] \\ &= N^2\left[\psi(N+1) - 2\psi(N) + \psi(N-1)\right].\end{aligned} \tag{A.4}$$

Now define

$$S(\mathcal{Z}) = s - \int_{\mathcal{Z}_{t^\star}}^{\mathcal{Z}} \frac{2nL_{loc}}{c_g\sqrt{1-c_g^2K^2}}d\mathcal{Z}' \quad \text{and} \quad X(\mathcal{Z}) = \chi - \int_{\mathcal{Z}_{t^\star}}^{\mathcal{Z}} \frac{2nL_{loc}c_gK}{\sqrt{1-c_g^2K^2}}d\mathcal{Z}', \tag{A.5}$$

and note that the joint process $\{n(\mathcal{Z}), S(\mathcal{Z}), X(\mathcal{Z})\}_{\mathcal{Z}\geq\mathcal{Z}'}$ is Markovian, with infinitesimal generator

$$\begin{aligned}
\tilde{\mathbb{G}}\psi(N,s,\chi) &= \lim_{\eta\to 0}\frac{1}{\eta}\left[E\left\{\psi\left(n(\mathcal{Z}+\eta), S(\mathcal{Z}+\eta), X(\mathcal{Z}+\eta)\right)|n(\mathcal{Z})=N, S(\mathcal{Z})=s, X(\mathcal{Z})=\chi\right\} - \psi(N,s,\chi)\right] \\
&= \lim_{\eta\to 0}\frac{1}{\eta}\left\{\left[\psi(N+1,s,\chi)+\psi(N-1,s,\chi)\right]N^2\eta + \psi\left(N, s-\frac{2\eta NL_{loc}}{c_g\sqrt{1-c_g^2K^2}}, \chi - \frac{2\eta NL_{loc}c_gK}{\sqrt{1-c_g^2K^2}}\right)\right. \\
&\qquad \left.\times\left(1-2N^2\eta\right) + o(\eta) - \psi(N,s,\chi)\right\} \\
&= \left\{\mathbb{G} - 2N\left[\frac{L_{loc}}{c_g\sqrt{1-c_g^2K^2}}\frac{\partial}{\partial s} + \frac{L_{loc}c_gK}{\sqrt{1-c_g^2K^2}}\frac{\partial}{\partial\chi}\right]\right\}\psi(N,s,\chi).
\end{aligned}$$

The solution of (A.3) is given by the Feynman-Kac formula [11]

$$\begin{aligned}
W_N(\omega,K,s,\chi,z(\mathcal{Z})) &= E\left\{W_{n(\mathcal{Z})}\left(\omega,K,S(\mathcal{Z}),X(\mathcal{Z}),\mathcal{Z}_{t^\star}\right)|n(\mathcal{Z}_{t^\star})=N, S(\mathcal{Z}_{t^\star})=s, X(\mathcal{Z}_{t^\star})=\chi\right\} \\
&= E\left\{\delta_{0,n(\mathcal{Z})}\delta\left[s-\int_{\mathcal{Z}_{t^\star}}^{\mathcal{Z}}\frac{2nL_{loc}}{c_g\sqrt{1-c_g^2K^2}}d\mathcal{Z}'\right]\delta\left[\chi-\int_{\mathcal{Z}_{t^\star}}^{\mathcal{Z}}\frac{2nL_{loc}c_gK}{\sqrt{1-c_g^2K^2}}d\mathcal{Z}'\right]\middle| n(\mathcal{Z}_{t^\star})=N\right\},
\end{aligned}$$

and the result stated in Lemma 3.4 follows after returning to the depth variable z,

$$W_N(\omega,K,s,\chi,z) = E_N\left\{\delta_{0,n(\mathcal{Z}(z))}\delta\left[s-\int_{-\mathcal{L}_{t^\star}}^{z}\frac{2n(\mathcal{Z}(z'))}{c\sqrt{1-c^2K^2}}dz'\right]\delta\left[\chi-\int_{-\mathcal{L}_{t^\star}}^{z}\frac{2n(\mathcal{Z}(z')cK}{\sqrt{1-c^2K^2}}dz'\right]\right\}. \tag{A.6}$$

A.1. Homogeneous background. In the case $c(z)=c_o$, (A.6) simplifies to

$$W_N(\omega,K,s,\chi,z) = E_N\left\{\delta_{0,n(\mathcal{Z}(z))}\delta\left[s-\frac{2}{c_o\sqrt{1-c_o^2K^2}}\int_{-\mathcal{L}_{t^\star}}^{z}n(\mathcal{Z}(z'))dz'\right]\right\}\delta\left[\chi-Kc_o^2s\right], \tag{A.7}$$

as we remarked in section 3.3. We are interested in evaluating W_N at the surface $z=0$. As we explained in section 3.3, $W_N(\omega,K,s,\chi,0)$ is not affected by the precise choice of $t^\star$, as long as we observe it at times s that are smaller than $t^\star$. This means that we may let $t^\star\to\infty$ or, equivalently, $\mathcal{L}_{t^\star}\to\infty$ and $\mathcal{Z}_{t^\star}\to-\infty$.

To take the limit, it is convenient to shift coordinates and introduce a new process

$$m(\xi) = n(\mathcal{Z}_{t^\star}+\xi), \quad \xi\in[0,-\mathcal{Z}_{t^\star}], \tag{A.8}$$

where

$$\xi(z) = \mathcal{Z}(z) - \mathcal{Z}_{t^\star} = \int_{-\mathcal{L}_{t^\star}}^{z}\frac{dz'}{L_{loc}(\omega,c_o,z')} = \frac{\omega^2 l}{4c_o^2(1-c_o^2K^2)}(z+\mathcal{L}_{t^\star}), \quad -\mathcal{L}_{t^\star}<z<0. \tag{A.9}$$

The new process satisfies the boundary conditions

$$m(0) = n(\mathcal{Z}_{t^\star}) = N \quad \text{and} \quad m(-\mathcal{Z}_{t^\star}) = n(0) \tag{A.10}$$

and we use it to define the random variable

$$\nu_N^{t^\star} = \frac{2}{c_o\sqrt{1-c_o^2K^2}}\int_{-\mathcal{L}_{t^\star}}^{0}n(\mathcal{Z}(z'))dz' = \frac{2}{c_o\sqrt{1-c_o^2K^2}}\int_{-\mathcal{L}_{t^\star}}^{0}m(\xi(z'))dz'. \tag{A.11}$$

Now we can let $t^\star \to \infty$, so that ξ is in the half space $[0,\infty)$. The process $\{m(\xi)\}_{\xi\geq 0}$ is recurrent [18], which means that $m(\xi)$ always reaches the absorbing state 0 for some bounded, (random) value of ξ. Thus, (A.11) has a limit

$$\nu_N = \lim_{t^\star\to\infty} \nu_N^{t^\star}, \tag{A.12}$$

and $W_N(\omega, K, s, \chi, 0)$ is given by

$$W_N(\omega, K, s, \chi, 0) = E\left\{\delta\left[s-\nu_N\right]|m(0)=N\right\}\delta\left[\chi - Kc_o^2 s\right]. \tag{A.13}$$

It remains to compute

$$f_{\nu_N}(s) = E\left\{\delta\left[s-\nu_N\right]|m(0)=N\right\}, \tag{A.14}$$

the probability density function of ν_N.

The density $f_{\nu_N}(s)$ follows from the Feynman-Kac formula [11], as before. Here we need only the process $S(\xi)$, which is basically the same as that in (A.5), except that it depends on the shifted coordinate ξ. To avoid singularities, we compute first the cumulative distribution $\mathcal{F}_{\nu_N}(s) = \int_0^s f_{\nu_N}(t)dt$, which satisfies

$$\begin{aligned}\frac{2NL_{loc}}{c_o\sqrt{1-c_o^2K^2}}\frac{\partial \mathcal{F}_{\nu_N}}{\partial s} &= N^2\left(\mathcal{F}_{\nu_{N+1}} - 2\mathcal{F}_{\nu_N} + \mathcal{F}_{\nu_{N-1}}\right), \quad s>0,\\ \mathcal{F}_{\nu_N}(0) &= \delta_{0,N}.\end{aligned} \tag{A.15}$$

This simple equation can be solved explicitly, and we obtain

$$\mathcal{F}_{\nu_N}(s) = \left[\frac{\tilde{s}}{2+\tilde{s}}\right]^N 1_{[0,\infty)}(s), \quad \tilde{s} = \frac{\omega^2 l s}{4c_o\sqrt{1-c_o^2K^2}}, \tag{A.16}$$

where $1_{[0,\infty)}(s)$ is the Heaviside step function. The result

$$E\left\{\delta[s-\nu_N]|m(0)=N\right\} = f_{\nu_N}(s) = \frac{\omega^2 lN}{2c_o\sqrt{1-c_o^2K^2}}\frac{\tilde{s}^{N-1}}{(2+\tilde{s})^{N+1}}1_{[0,\infty)}(s) \tag{A.17}$$

follows from (A.13), after differentiating (A.16) with respect to s. Furthermore, we have from (A.12) and (A.17) that in the particular case $N=1$,

$$W_1(\omega, K, s, \chi, 0) = \frac{\omega^2 lN}{2c_o\sqrt{1-c_o^2K^2}}\frac{1_{[0,\infty)}(s)}{(2+\tilde{s})^2}\delta[\chi - Kc_o^2 s]. \tag{A.18}$$

This is the formula used in the proof of Theorem 3.3.

REFERENCES

[1] M. Asch, W. Kohler, G. Papanicolaou, M. Postel, and B. White, *Frequency content of randomly scattered signals*, SIAM Review, 33 (1991), pp. 519–625.

[2] E. Bécache, P. Joly, and C. Tsogka, *Etude d'un nouvel élément fini mixte permettant la condensation de masse*, C. R. Acad. Sci. Paris Sér. I Math., 324 (1997), pp. 1281–1286.

[3] ———, *An analysis of new mixed finite elements for the approximation of wave propagation problems*, SIAM J. Numer. Anal., 37 (2000), pp. 1053–1084.

[4] Biondo Biondi, *3D Seismic Imaging*, no. 14 in Investigations in Geophysics, Society of Exploration Geophysicists, Tulsa, 2006.

[5] G. Blakenship and G. Papanicolaou, *Stability and control of systems with white-band noise disturbances*, SIAM J. Appl. Math, 34 (1978), pp. 437–476.
[6] N. Bleistein, J.K. Cohen, and J.W. Stockwell Jr., *Mathematics of multidimensional seismic imaging, migration, and inversion*, Springer, New York, 2001.
[7] L Borcea, *Robust inteferometric imaging in random media*, in The Radon transform, inverse problems, and tomography, no. 63 in Proc. Sympos. Appl. Math., Providence, RI, 2006, Amer. Math. Soc., pp. 129–156.
[8] L. Borcea, F. González del Cueto, G. Papanicolaou, and C. Tsogka, *Layer filtering for imaging and velocity estimation*, SIAM Multiscale Analysis, (submitted 2008).
[9] L. Borcea, G. Papanicolaou, and C. Tsogka, *Coherent interferometry in finely layered random media*, SIAM Multiscale Modeling and Simulation, 5 (2006), pp. 62–83.
[10] B. Borden, *Mathematical problems in radar inverse scattering*, Inverse Problems, 19 (2002), pp. R1–R28.
[11] L. Breiman, *Probability*, SIAM, second printing ed., 1993.
[12] J. Carazzone and W. Symes, *Velocity inversion by differential semblance optimization*, Geophysics, 56 (1991).
[13] J. F. Claerbout, *Fundamentals of geophysical data processing : with applications to petroleum prospecting*, CA : Blackwell Scientific Publications, Palo Alto, 1985.
[14] J. F. Claerbout, *Earth soundings analysis: Processing versus inversion*, Blackwell Scientific Publications, Inc., 1992.
[15] J. F. Clouet and J. P. Fouque, *Spreading of a pulse travelling in random media*, Annals of Applied Probability, Vol.4, No.4, (1994).
[16] F. Collino, P. Joly, and F. Millot, *Perfectly matched absorbing layers for the paraxial equations*, J. Computational Physics, 131 (1996), pp. 164–180.
[17] J.C. Curlander and R.N. McDonough, *Synthetic Aperture Radar*, Wiley, New York, 1991.
[18] W. Feller, *An introduction to probability theory and its applications*, vol. 1, John Wiley & Sons, 3 ed., 1968.
[19] S Fomel, *Application of plane-wave destruction filters*, Geophysics, 67 (2002), pp. 1946–1960.
[20] S. Fomel, E. Landa, and M. Turham Taner, *Poststack velocity analysis by separation and imaging of seismic diffractors*, Geophysics, 72 (2007), pp. U89–U94.
[21] J.-P. Fouque, J. Garnier, G. Papanicolaou, and K. Sølna, *Wave Propagation and Time Reversal in Randomly Layered Media*, Springer, April 2007.
[22] R.F. O'Doherty and N. A. Anstey, *Reflections on amplitudes*, Geophysical Prospecting, 19 (1971), pp. 430–458.
[23] G. Papanicolaou, D. W. Stoock, and S. R. S. Varadhan, *Martingale approach to some limit theorems*, in Statistical Mechanics and Dynamical Systems, Duke turbulence conference, D. Ruelle, ed., Duke Univ. Math. Series III, part IV, 1976, pp. 1–120.
[24] K. Sølna and G. Papanicolaou, *Ray theory for a locally layered random medium*, Waves Random Media, (2000).
[25] W. Symes, *All stationary points of differential semblance are asymptotic global minimizers: Layered acoustics*, Stanford Exploration Project, (1999), pp. 71–92. Report 100.
[26] B. White, P. Sheng, and B. Nair, *Localization and backscattering spectrum of seismic waves in stratified lithology*, Geophysics, (1990), pp. 1158–1165.